EDIVAL-AGENT: AN OBJECT-CENTRIC FRAMEWORK FOR AUTOMATED, SCALABLE, FINE-GRAINED EVALUATION OF MULTI-TURN EDITING

Tianyu Chen[1,*], **Yasi Zhang**[2,*], **Zhi Zhang**[2], **Peiyu Yu**[2], **Shu Wang**[2], **Zhendong Wang**[3], **Kevin Lin**[3], **Xiaofei Wang**[3], **Zhengyuan Yang**[3], **Linjie Li**[3], **Chung-Ching Lin**[3], **Jianwen Xie**[4] **Oscar Leong**[2,†], **Lijuan Wang**[3,†], **Ying Nian Wu**[2,†], **Mingyuan Zhou**[1,3,†]
[1]University of Texas at Austin [2]University of California, Los Angeles [3]Microsoft [4]Lambda, Inc

ABSTRACT

Instruction-based image editing has advanced rapidly, yet reliable and interpretable evaluation remains a bottleneck. Current protocols either (i) depend on paired reference images—resulting in limited coverage and inheriting biases from prior generative models—or (ii) rely *solely* on zero-shot vision–language models (VLMs), whose prompt-based assessments of instruction following, content consistency, and visual quality are often imprecise.

To address this, we introduce **EdiVal-Agent** , an automated, scalable, and fine-grained evaluation framework for multi-turn instruction-based editing from an object-centric perspective, supported by a suite of expert tools. Given an image, **EdiVal-Agent** first decomposes it into semantically meaningful objects, then synthesizes diverse, context-aware editing instructions. For evaluation, it integrates VLMs with open-vocabulary object detectors to assess instruction following, uses semantic-level feature extractors to evaluate content consistency, and leverages human preference models to judge visual quality. We show that combining VLMs with object detectors yields stronger agreement with human judgments in instruction-following evaluation compared to using VLMs alone and CLIP-based metrics. Furthermore, the pipeline's modular design allows future tools to be seamlessly integrated, enhancing evaluation accuracy over time.

Instantiating this pipeline, we build **EdiVal-Bench**, a multi-turn editing benchmark covering 9 instruction types and 11 state-of-the-art editing models spanning autoregressive (AR), flow-matching, and diffusion paradigms. Our analysis shows that *Nano Banana* achieves the best overall balance of instruction following and content consistency while maintaining surprisingly low latency; *GPT-Image-1* exhibits the strongest instruction following across turns but ranks among the lowest in content consistency and has high latency; AR models substantially outperform non-AR models in multi-turn editing by better preserving contextual coherence; and *Qwen-Image-Edit* is strong on the first turn but degrades in later turns due to exposure bias. We demonstrate that **EdiVal-Agent** can be used to identify existing failure modes, thereby informing the development of the next generation of editing models. Project page: `https://tianyucodings.github.io/EdiVAL-page/`

1 INTRODUCTION

What truly defines the success of an instruction-based image editor? At its core, editing requires making targeted, instruction-driven changes while preserving contextual consistency and perceptual realism—often across multiple refinement turns. Yet current evaluation practice struggles to capture this multifaceted objective.

[*]Equal contribution. Correspondonce to `tianyuchen@utexas.edu` and `yasminzhang@ucla.edu`.
[†]Equal advising.

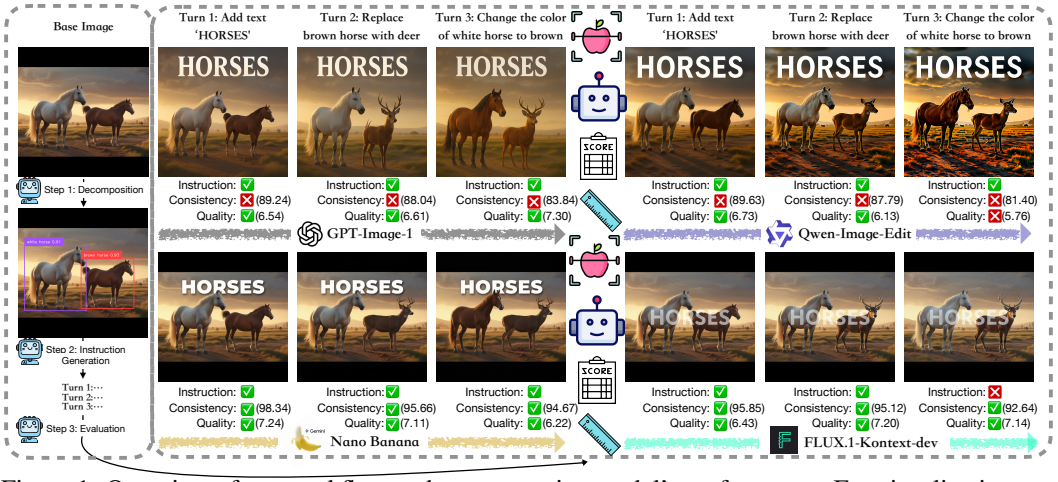

Figure 1: Overview of our workflow and representative model's performance. For visualization, we adopt two thresholds: a consistency score of at least 90 and a visual quality score of at least 6. Details of the automated evaluation pipeline are provided in Figure 2 and Section 3. In multi-turn editing, models exhibit distinct weaknesses: *GPT-Image-1* struggles with content consistency, *Qwen-Image-Edit* underperforms in both visual quality and content consistency, and *FLUX.1-Kontext-dev* lags in instruction following, whereas *Nano Banana* shows no single dominant weakness. A comprehensive analysis is presented in Sec. 5 and Tab. 2.

When ground-truth edited images are available, a common strategy is to compare model outputs against these references Zhang et al. (2023); Zhao et al. (2024); Yu et al. (2025); Sheynin et al. (2024). Typical metrics include pixel-level distances (e.g., L1/L2) and semantic similarities (e.g., DINO Caron et al. (2021) and CLIP Radford et al. (2021)). While informative, such metrics suffer from two structural issues: (i) the space of acceptable edits is inherently large, whereas a single reference provides only one realization; and (ii) references are frequently synthesized by existing editing models (e.g., Prompt-to-Prompt Hertz et al. (2023), SDXL Podell et al. (2024), DALLE-2 Ramesh et al. (2022)), thereby importing their biases and limitations into the evaluation itself. Consequently, high reference similarity does not necessarily imply faithful instruction following, preservation of irrelevant content, or aesthetically plausible outcomes.

A complementary line of work employs VLMs as interpretable evaluators—for example, VIEScore Ku et al. (2023), HQ-Edit Hui et al. (2024), and Complex-Edit Yang et al. (2025)—and queries VLMs about specific aspects of an edit. While VLMs offer holistic, language-mediated judgments, they remain insufficient for precise editing assessment for several reasons. First, for instruction-following evaluation, they are notoriously poor at spatial reasoning Zhang et al. (2025b); Chen et al. (2024); Chang et al. (2025) and are prone to object hallucinations in existence, category, attributes, and relations Bai et al. (2024). These issues together undermine their ability to assess common object-related edit instructions. Second, they have limited sensitivity to pixel-level changes and frequently miss subtle, localized modifications Vo et al. (2025) (e.g., fine structures, small attribute shifts, etc.), which are crucial for evaluating content consistency. Third, since they are predominantly pretrained on natural images rather than synthetic generations, their priors are miscalibrated for artifacts and aesthetics, leading to failures in detecting common generative defects (e.g., extra fingers) and in modeling perceptual "naturalness" Liang et al. (2024); Xu et al. (2023); Ma et al. (2025a), which humans are sensitive to. Consequently, VLM-only scoring lacks the precision and reliability required for fine-grained evaluation across instruction following, content consistency, and visual quality.

To address these challenges, we introduce **EdiVal-Agent**: an automated, scalable, and fine-grained evaluation agent for multi-turn instruction-based image editing from an object-centric perspective, supported by a suite of expert tools. As shown in Fig. 2, **EdiVal-Agent** first decomposes images into semantically meaningful components and identifies their contextual relationships. It then generates diverse and proper editing scenarios at scale, which are based on the initial analysis. Finally, it systematically evaluates editing model outputs from multiple axes, specifically by integrating VLMs with open-vocabulary object detectors to assess instruction following, using semantic-level feature

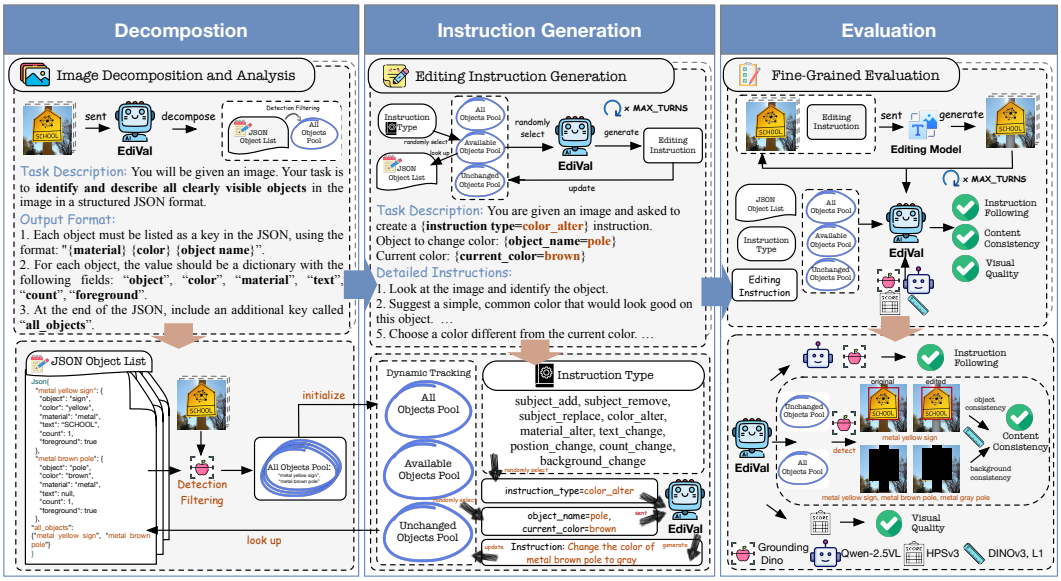

Figure 2: Framework of **EdiVal-Agent**. It first decomposes images into semantically meaningful objects, such as *metal yellow sign* and *metal brown pole*, and identifies their contextual relationships, e.g., they are both in *foreground*. It then generates diverse and proper editing scenarios at scale which are based on the initial analysis, e.g., *Change the color of metal brown pole to gray*. Finally, it systematically evaluates editing model outputs from multiple axes, including instruction following, content consistency, and visual quality, specifically by integrating VLMs (Qwen2.5-VL) with open-vocabulary object detectors (Grouding-DINO) to assess instruction following, using semantic-level feature extractors (DINOv3) and pixel-level metrics (L_1 distance) to evaluate content consistency, and leveraging human preference models (HPSv3) to judge visual quality. Our agentic pipeline is agnostic to the expert tools used and can be readily enhanced with more advanced tools in the future.

extractors to evaluate content consistency, and leveraging human preference models to judge visual quality. We show that combining VLMs with object detectors yields stronger agreement with human judgments in instruction-following evaluation compared to thresholded CLIP directional (CLIP_dir) scores Gal et al. (2022) and using VLMs alone, as evidenced in Sec. 4. Note that the full evaluation process, from evaluation instruction creation to evaluation metrics, is fully automated, without human intervention. This results in a scalable pipeline that can be easily expanded.

Instantiating the agentic pipeline, we curate a new multi-turn image editing benchmark, **EdiVal-Bench**, featuring 9 instruction types and 11 existing editing models—spanning autoregressive (AR), flow-matching, and diffusion paradigms, across both closed- and open-source systems—conduct fine-grained analyses, and draw actionable insights. Empirically, as demonstrated in Fig. 1 and Tab. 2, *GPT-Image-1* excels at instruction following yet ranks near the bottom in content consistency, whereas *Nano Banana* performs strongly on both axes. Besides, recently released open-sourced models like *Qwen-Image-Edit* significantly degrade in visual quality when editing turns increase, and fails to maintain consistency with the base image, while *FLUX.1-Kontext-dev* lags in instruction following. We further study editing behavior differences between AR and non-AR models in the multi-turn setting, and contrast multi-turn editing with complex single-shot prompts Yang et al. (2025), highlighting complementary strengths and failure modes. We hope that our agent pipeline, benchmark, and analyses accelerate the transition of multi-turn editing toward practical applications.

Key contributions. 1) *Agent:* **EdiVal-Agent** is a fully automated, scalable evaluator that performs object-centric decomposition, generates multi-turn editing instructions, and integrates VLM reasoning with symbolic pixel- and semantic-level metrics via grounding tools; 2) *Benchmark:* using **EdiVal-Agent**, we build **EdiVal-Bench** with 1,716 instructions across 9 types and 3 turns on 572 real-world images; 3) *Human agreement:* **EdiVal-Agent** achieves 81.3% agreement with human ratings in instruction following, outperforming zero-shot VLMs and CLIP-based methods; 4) *Evaluation:* we assess 11 editors (diffusion, flow-matching, autoregressive) along instruction following, content consistency, and visual quality; 5) *Insights:* AR models better preserve contextual coherence

and instruction accuracy across turns, while non-AR models exhibit exposure bias and cumulative degradation; 6) *Artifacts & settings:* we reveal luminance drift across turns, and contrast multi-turn against complex single-shot editing to delineate strengths and weaknesses across model families.

2 Related Work

Instruction-based editing models. InstructPix2Pix (IP2P) Brooks et al. (2023) introduced a two-stage recipe that converts a text-to-image diffusion model Rombach et al. (2022); Zhang et al. (2025a) into an editor: (i) synthesize paired editing data using Stable Diffusion Rombach et al. (2022) and training-free techniques such as Prompt-to-Prompt Hertz et al. (2023); (ii) fine-tune the diffusion model on these pairs. Subsequent systems—MagicBrush Zhang et al. (2023), UltraEdit Zhao et al. (2024), and AnyEdit Yu et al. (2025)—scale this paradigm to large, fine-grained real-image editing. More recent work (e.g., OmniGen Xiao et al. (2025); Wu et al. (2025b), Step1X-Edit Liu et al. (2025), FLUX.1 Kontext Labs et al. (2025), and Qwen-Image-Edit Wu et al. (2025a)) adopts task-aware architectures and increasingly leverages flow matching Liu et al. (2022); Lipman et al. (2022); Zhang et al. (2024).

A complementary line explores autoregressive (AR) editors such as Gemini 2.0 Flash Image Gemini2 (2025), Gemini 2.5 Flash Image ("Nano Banana") Deepmind (2025), and GPT-Image-1 OpenAI (2025). These models enable **in-context multi-turn editing**: users iteratively refine an image within a conversational interface, with the model maintaining a coherent editing history. To our knowledge, we provide the first systematic comparison of in-context multi-turn AR editing versus context-free multi-turn editing with non-AR models across instruction following, content consistency, and visual quality.

Editing evaluation. Early evaluations (e.g., Brooks et al. (2023)) rely on CLIP-based similarity Radford et al. (2021), including directional variants Gal et al. (2022), to approximate editing quality. However, CLIP emphasizes semantic alignment and is less sensitive to fine, pixel-level changes. When ground-truth edited images exist, it is natural to compare model outputs against references using pixel distances (L_1) and semantic similarities (DINO Caron et al. (2021), CLIP Radford et al. (2021)) Zhang et al. (2023); Zhao et al. (2024); Yu et al. (2025); Sheynin et al. (2024). Yet references are imperfect: the space of valid edits is inherently multimodal, while a single reference captures only one realization; moreover, many references are themselves synthesized by prior editors (e.g., Prompt-to-Prompt Hertz et al. (2023), SDXL Podell et al. (2024), DALLE-2 Ramesh et al. (2022)), importing their biases into evaluation.

Recent work relies exclusively on VLMs as interpretable judges—e.g., VIEScore Ku et al. (2023), HQ-Edit Hui et al. (2024), and Complex-Edit Yang et al. (2025)—by querying models such as GPT-4o OpenAI (2025) about specific aspects of an edit. While VLMs offer holistic, language-mediated assessments, they are insufficient on their own: they are notoriously poor at spatial reasoning Zhang et al. (2025b); Cheng et al. (2024); Chen et al. (2024); Qharabagh et al. (2024); Chang et al. (2025) and are prone to object hallucinations in existence, category, attributes, and relations Bai et al. (2024); they have limited sensitivity to pixel-level changes and frequently miss subtle, localized modifications Vo et al. (2025) (e.g., fine structures, small attribute shifts, etc.), which are crucial for evaluating content consistency; they are miscalibrated for artifacts and aesthetics Liang et al. (2024); Xu et al. (2023); Ma et al. (2025a), which humans are sensitive to. Our approach, **EdiVal-Agent**, addresses these gaps by integrating VLM-based reasoning with grounding tools, symbolic, object-centric pixel- and semantic-level tools, and human preference models, yielding a precise and interpretable evaluation of instruction-based editing.

Editing tasks. We consider three settings: (i) **Single-turn vs. multi-turn.** Multi-turn editing Zhang et al. (2023); Zhao et al. (2024) is more demanding than single-turn, as the model must maintain consistency across sequential instructions. In contrast to *context-free* multi-turn pipelines (each turn consumes the previous image and the next instruction), AR models Gemini2 (2025); Deepmind (2025); OpenAI (2025) support *in-context* multi-turn editing by conditioning on the full conversational history. (ii) **Complex single-shot vs. multi-turn.** Following Yang et al. (2025), a sequence of edits can be concatenated into a single complex prompt and executed in one pass; we compare this setting to genuine multi-turn editing. (iii) **Other tasks.** We focus on instruction-based editing, the most common regime; other scenarios (e.g., prompt-to-prompt/caption-to-caption

Hertz et al. (2023)) are outside our scope. To the best of our knowledge, this paper offers the first comprehensive comparison covering single-turn, multi-turn, and complex single-shot editing within a unified framework.

3 EDIVAL-AGENT

3.1 OVERVIEW

EdiVal-Agent is a fully automated, scalable framework for evaluating instruction-based image editing from a symbolic, object-centric perspective, as illustrated in Fig. 2. The pipeline comprises three stages: (1) *Decomposition* uses a VLM (e.g., GPT-4o; other VLMs are viable alternatives) to extract structured, object-level descriptions—objects, attributes, and relations—enabling symbolic reasoning; (2) *Instruction Generation* produces multi-turn, diverse, compositional prompts by maintaining an explicit object pool and sampling from nine instruction types spanning subject-, attribute-, relational-, text-, count-, and global-level edits; (3) *Evaluation* scores edited images along *Instruction Following*, *Content Consistency*, and *Visual Quality*, combining Grounding-DINO Liu et al. (2024a), Qwen-VL 2.5 Yang et al. (2024), DINOv3 Siméoni et al. (2025), pixel-wise L_1, and the HPSv3 quality scorer Ma et al. (2025a). Our agentic pipeline is agnostic to the agent VLM/expert tools used and can be readily enhanced with more advanced tools in the future.

3.2 STEP 1: DECOMPOSITION

Given an image, a VLM-based agent parses clearly visible foreground objects and returns per-object JSON with fields `object`, `color`, `material`, `text`, `count`, and a boolean `foreground`. Names follow `"{material} {color} {object}"`; unknown fields are omitted; person identity is never recorded (only wearables/accessories). Example: `{"metal yellow sign": {"object":"sign","color":"yellow","material":"metal","text":"SCHOOL","count":1,"foreground":true}}`. An aggregated `all_objects` string concisely lists objects (e.g., "metal yellow sign . metal brown pole"). We apply this stage to GEdit-Bench Liu et al. (2025) (606 images), exclude 34 images with sensitive personal content, and retain 572 images. After extraction, Grounding-DINO validates objects and detects bounding boxes; only reliable detections are kept to seed instruction generation and evaluation. The filtered objects are stored in the `All_Objects_Pool` and later used to initialize three distinct object pools that dynamically track the evolving state of instruction generation.

3.3 STEP 2: INSTRUCTION GENERATION

From the decomposed scene, the agent generates multi-turn edits that are grounded in the current object state. The instruction taxonomy (nine types; six categories) appears in Table 1. We maintain three evolving pools at turn t: $\mathcal{P}_t^{\text{all}}$ (all objects ever present), $\mathcal{P}_t^{\text{unch}}$ (original objects not edited up to t), and $\mathcal{P}_t^{\text{avail}}$ (objects currently editable). With a turn budget `MAX_TURNS`, at each turn the agent (i) selects a type—defaulting to `subject_add` if $\mathcal{P}_t^{\text{avail}} = \emptyset$, otherwise sampling a type not yet used in the chain; (ii) selects object(s) from $\mathcal{P}_t^{\text{avail}}$; (iii) emits a natural-language instruction via GPT-4o referencing those objects and the scene state; and (iv) updates $\mathcal{P}_{t+1}^{\text{all}}$, $\mathcal{P}_{t+1}^{\text{avail}}$, and $\mathcal{P}_{t+1}^{\text{unch}}$ according to the intended edit. When a `background_change` edit applies at turn t, background-consistency scoring is disabled since this turn, and we append "make {`objects_in_foreground`} unchanged" to the instruction to preserve object-level comparability, where $\texttt{objects\_in\_foreground} = \{ o \in P_t^{\text{avail}} : o.\texttt{foreground} = \texttt{true} \}$. The loop is adaptive by expanding/contracting $\mathcal{P}_t^{\text{avail}}$ and naturally compositional. Our default sets `MAX_TURNS`$= 3$ (In our implementation, each turn is assigned a distinct instruction type.), though longer chains are easily obtained by allowing repetition or adding types.

3.4 STEP 3: EVALUATION

Instruction Following separates types by evaluability. Symbolically verifiable types—`subject_add`, `subject_remove`, `subject_replace`, `position_change`, `count_change`—are *solely* checked with **Grounding-DINO** Liu et al. (2024b) using prompts derived from the instruction and object descriptors; compliance uses detection confidence,

Table 1: **Instruction types in EdiVal-Bench** created by **EdiVal-Agent**, grouped by semantic category. Counts are shown per turn (T1–T3).

Category	Instruction Type	Example Instruction	T1	T2	T3	Total
Subject-centric	`subject_add`	Add bench on the left of metal red fire hydrant.	67	77	93	237
	`subject_remove`	Remove wooden brown door.	75	69	61	205
	`subject_replace`	Replace stone gray railing with wooden fence.	54	57	55	166
Attribute-centric	`color_alter`	Change the color of metal white airplane to blue.	56	73	57	186
	`material_alter`	Change the material of plastic black pen to metal.	66	50	72	188
Text-related	`text_change`	Replace the text 'BEARS CONTROL' on cotton black cap with 'WILD PATH'.	64	70	54	188
Relational	`position_change`	Change the position of ceramic white cup to right of plastic white laptop.	52	63	48	163
Counting	`count_change`	Change the count of fur brown bear to 3.	73	58	60	191
Global	`background_change`	Change the background to forest, remain the brown fur bear unchanged.	65	55	72	192

counts, and geometry (existence and relative positions), following GENEVAL Ghosh et al. (2023) and T2I-CompBench Huang et al. (2023). Semantically verifiable types—`color_alter`, `material_alter`, `text_change`, and `background_change`—are evaluated with **Qwen2.5-VL** Yang et al. (2024) using instruction-specific templates (See details in Appendix), applied to detector-guided (i.e., **Grounding DINO**) object crops to focus on the edited regions. The multiturn instruction following accuracy aggregates per-instruction pass/fail along the chain (see details in Appendix).

Content Consistency assesses whether non-target content is preserved at semantic and pixel levels. Let $\mathcal{B}^t$ denote the **Grounding-DINO** detections at turn t; define object and background regions as Ω^t_{obj} and Ω^t_{bg}. For objects, we crop each element of $\mathcal{P}^{\text{unch}}_t$ from I^0 and I^t and compute **DINOv3** cosine similarity $s^{\text{obj}} = \cos\big(\phi(I^0_{\text{obj}}), \phi(I^t_{\text{obj}})\big)$ and a normalized pixel metric $q^{\text{obj}} = 1 - \|I^0_{\text{obj}} - I^t_{\text{obj}}\|_1/Z$, averaged over unchanged objects (larger is better). Here $\|\cdot\|_1$ sums over all pixels and channels within the crop, and Z normalizes the pixelwise $\mathbf{L}_1$ **distance** to $[0, 1]$; for a region with C channels, $|\Omega|$ pixels, and per-channel dynamic range Δ (e.g., $\Delta = 255$ for 8-bit RGB or $\Delta = 1$ for $[0, 1]$-scaled floats), we set $Z = C\,|\Omega|\,\Delta$. For background, we mask $\mathcal{B}^t$ and compute the same two measures over Ω^0_{bg} versus Ω^t_{bg}; if a `background_change` occurs at turn t, background scoring is disabled thereafter and omitted from the combined score.

Visual Quality is measured using Human Preference Score v3 (**HPSv3**) Ma et al. (2025b), which yields scores aligned with human preference and captures both aesthetics and visual plausibility for image synthesis. We avoid general-purpose VLMs for aesthetic judgments because they are biased toward real-image semantics and less sensitive to synthesis artifacts. We also observe systematic overexposure in some models under multiturn editing; to quantify this effect, we also compute **low-level exposure statistics** (e.g., luminance percentiles).

Design Scope and Limitations. We omit `style_change` from the current taxonomy. Open-vocabulary detectors optimized for natural images (e.g., Grounding-DINO) generalize poorly to strongly stylized domains, undermining reliable symbolic verification. Extending **EdiVal-Agent** with style-aware recognition is promising future work. After language-based extraction, we validate objects with Grounding-DINO, pruning low-confidence or ambiguous detections, and canonicalizing names to a uniform schema. This stabilizes the object pools, reduces error propagation during instruction generation, and tightens the coupling between symbolic references and detector-visible entities. The pipeline is fully automated and scales linearly with dataset size; privacy is enforced by excluding sensitive images at ingestion and never recording identities—only attributes of visible clothing and accessories.

4 Measuring Human Agreement

Setup. We conduct human study on edits made by four exemplary models, Step1X-Edit, AnyEdit, Gemini-Flash 2.0 and Flux.1-Kontext-dev, on **EdiVal-Bench**, generated by **EdiVal-Agent** as described in Section 3.3. For each edit, we collect two human ratings for each edit, yielding a total

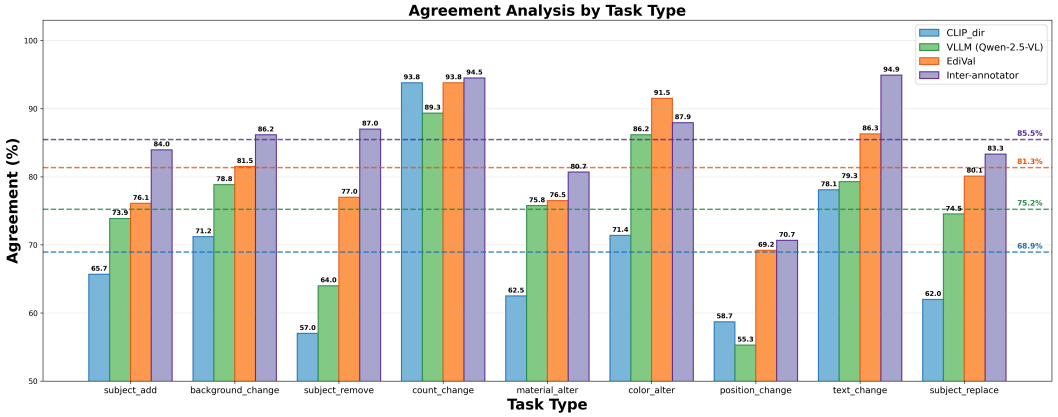

Figure 3: Results of human agreement. Dashed lines represent the average accuracy of each method. **EdiVal-Agent** achieves 81.3% human agreement accuracy, significantly outperforming the VLM (Qwen2.5-VL) at 75.2% and thresholded CLIP_dir at 65.4%. Note that the CLIP_dir threshold is tuned separately for each task. The inner-annotation baselines indicate the ceiling performance achievable by the tools.

of $572 \times 4 \times 2 = 4{,}576$ annotations. Raters were recruited online, each holding at least a bachelor's degree. During evaluation, they were shown the original image, the edited image, and the corresponding instruction. They were asked a binary question: *"Evaluate whether the edited image successfully follows the given instruction."*

Results. Figure 3 summarizes the findings. **EdiVal-Agent** achieves a human agreement accuracy of **81.3%**, significantly higher than VLM-only (*Qwen-2.5-VL*, 75.2%), CLIP_dir (65.4%), and other zero-shot VLMs. These results verify that integrating VLMs reasoning with object detection leads to better alignment with human judgment compared to existing methods. The inter-annotator's agreement rate (85.5%) indicates the best performance any evaluation tool can reach.

We attribute the improvement in instruction-following evaluation to two factors. First, for symbolically verifiable instruction types—`subject_add`, `subject_remove`, `subject_replace`, `position_change`, and `count_change`—**EdiVal-Agent** relies solely on Grounding-DINO. It determines the success of an edit by checking object presence/absence, the positions of object centers, and the number of bounding boxes. Results for `position_change` and `subject_remove` show that these fixed rules, combined with Grounding-DINO, can significantly outperform Qwen2.5-VL in edit evaluation. We hypothesize that errors in `position_change` stem from poor spatial reasoning, while failures in `subject_remove` are due to hallucinations regarding object existence. Second, semantically verifiable types—`color_alter`, `material_alter`, `text_change`, and `background_change`—are evaluated using **Qwen2.5-VL** combined with Grounding-DINO. The decomposition stage in **EdiVal-Agent** can supports evaluation by localizing text regions, enabling the LLM to reason more precisely about text edits. These findings demonstrate that **EdiVal-Agent** not only enhances interpretability but also improves the practical applicability of evaluation pipelines in real-world scenarios requiring human-like understanding.

5 Benchmarking Multi-turn Editing

Editing Models We evaluate three families of image editors: (i) diffusion-based models (InstructPix2Pix (IP2P), MagicBrush, UltraEdit, AnyEdit), (ii) flow-matching models (FLUX.1-Kontext-dev, Qwen-Image-Edit, Step1X-Edit, OmniGen), and (iii) autoregressive/regeneration models (Gemini 2.0 Flash, Nano Banana, and GPT-Image-1)[1].

EdiVal-Bench We evaluate all models on **EdiVal-Bench**, generated by **EdiVal-Agent** as described in Section 3.3. The source images are from GEdit-Bench Liu et al. (2025), which contains

[1]These models are closed-source and lack public technical reports. We label them "Autoregressive" because they are integrated into an autoregressive language model in the web UI.

606 real-world images. For safety, we exclude 34 images with sensitive personal content, yielding 572 images successfully decomposed by **EdiVal-Agent**. During instruction generation we set `MAX_TURNS=3`, producing 1,716 editing instructions spanning 9 types (Table 1). In short, every model is evaluated on the same images and the same instructions, using the same metrics.

Metrics As described in Section 3.4, we evaluate three complementary dimensions. First, *instruction following* α_i is the image-success rate at turn i — the fraction of images for which *all* edits up to and including turn i are successful. Second, *content consistency* captures the stability of unchanged objects and background across turns. Consistency is computed primarily using DINOv3 feature similarity for the object and background regions; we also report pixel-level L_1 distances as diagnostic statistics. Let κ_i denote the content-consistency score at turn i, defined as the mean of the object and background DINOv3 similarities. To summarize overall performance on these two dimensions, we combine with a geometric mean: $\textit{Overall} = \sqrt{\alpha_i \kappa_i}$, which favors models that achieve balanced gains in both instruction following and content preservation. Perceptual quality (e.g., aesthetics and luminance-based statistics) is reported separately and is *not* folded into *Overall*.

We evaluate multi-turn editing across a mix of closed- and open-source models. Unless noted, higher is better; latency is measured in seconds per image (lower is better). We first summarize overall trends and quantitative results (Section 5.1), then analyze instruction following (Section 5.2) and consistency (Section 5.3). We also assess perceptual quality using both learned human-preference scores and low-level statistics (Section 5.4). Finally, because multi-turn instructions can often be compressed into a single prompt, we compare multi-turn versus single-shot "complex" editing (Section 5.5).

5.1 Overall Results

Table 2: **Results of multi-turn editing.** Instruction following, content consistency, and overall across three sequential editing turns. *Overall* is the geometric mean of instruction following and content consistency. Best per column in **dark red**; second-best in lighter red. Latency is seconds per image (lower is better).

Technique	Model	Date	Latency (s/img)	Instruction Following			Content Consistency			Overall		
				T1	T2	T3	T1	T2	T3	T1	T2	T3
Autoregressive	Nano Banana	25.08.26	9.70	70.70	50.66	35.35	93.91	90.48	89.48	**81.48**	**67.70**	**56.24**
	GPT-Image-1	25.07.16	71.30	**73.12**	**54.89**	**38.35**	81.00	77.78	75.50	76.96	65.34	53.81
	Gemini 2.0 Flash	25.02.05	8.20	68.07	45.96	28.42	90.58	85.10	80.88	78.52	62.54	47.94
Flow Matching	Qwen-Image-Edit	25.08.04	115.08	72.90	44.06	22.55	84.22	80.52	77.98	78.36	59.56	41.93
	Step1X-Edit	25.04.25	20.42	61.89	34.97	17.83	92.76	88.52	85.21	75.77	55.64	38.98
	FLUX.1-Kontext-dev	25.06.25	29.21	59.97	32.69	16.61	**95.32**	**92.24**	**90.22**	75.61	54.91	38.71
	OmniGen	24.09.11	19.70	54.72	24.48	10.66	93.00	88.42	83.92	71.34	46.52	29.91
Diffusion	AnyEdit	24.11.24	3.93	41.07	16.32	7.22	86.42	78.91	70.10	59.58	35.89	22.50
	UltraEdit	24.07.07	3.15	51.37	17.70	6.36	86.80	84.50	82.40	66.78	38.67	22.89
	MagicBrush	23.06.16	4.08	42.31	15.73	4.90	86.96	81.26	76.86	60.66	35.75	19.41
	IP2P	23.12.15	4.09	37.41	10.66	2.80	76.85	68.36	60.30	53.62	26.99	12.99

Summary. Based on the data in Table 2, across three turns, *Nano Banana* offers the best speed–quality trade-off—highest *Overall* at T1/T2/T3 (81.48/67.70/56.24) with 9.7 s/img. *GPT-Image-1* delivers the strongest instruction following across turns, but its latency (71.3 s/img)[2] and weaker consistency leave it second in *Overall*; *Nano Banana* trails GPT-4o by only ∼4.2 (T2) and 3.0 (T3) points on instruction following. For consistency, *FLUX.1-Kontext-dev* leads across turns with *Nano Banana* close behind, whereas *GPT-Image-1* ranks second-to-last—consistent with more regenerative/restyling behavior that can erode pixel/feature stability despite aesthetic gains. *Gemini 2.0 Flash* is competitive at T1 (second-best *Overall*) but exhibits a steeper decline by T3. Among open-source systems, *Qwen-Image-Edit* is strongest at T1 (Overall 78.36) yet degrades rapidly with additional turns, likely due to exposure bias from single-turn training on real images and a short edit-history window that forces the model to operate on its own outputs, more evidence in Section 5.2 and 5.5.

[2]Closed-source latencies are measured in the provider's hosted web UI; open-source latencies on a single NVIDIA A100 GPU with default settings.

5.2 INSTRUCTION FOLLOWING

Marginal Task Success Rate. We analyze instruction-following ability across nine edit tasks. For a given turn, the *marginal task success rate* is the proportion of prompts for which the requested edit in that turn is successfully implemented. In contrast, the *instruction following* score reported in Table 2 corresponds to the *multi-turn task success rate* at turn i—the fraction of images for which all edits up to turn i are successful.

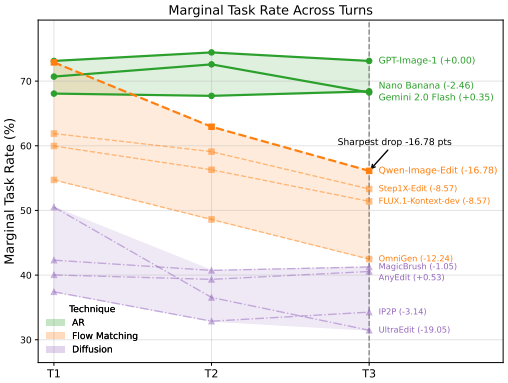

Figure 4: Marginal instruction-following across turns.

Figure 4 shows the evolution of per-turn performance. Models that are **AR** (autoregressive) and condition on the full editing history are relatively stable across turns: their marginal task success rates change only slightly between turns. By contrast, **non-AR** models with a very short history window (effectively conditioning only on the previous output) suffer substantial degradation in marginal task success, particularly for flow-matching style models.

A striking example is **Qwen-Image-Edit**. It is the strongest open-source system at turn 1 (Overall 78.36 vs. 81.48 for Nano Banana) but degrades much faster over subsequent turns. We hypothesize that this is primarily an *exposure bias* issue: many single-turn edit models are trained to operate on real images and ground-truth inputs, not on their own earlier outputs. When a model must operate on its own previous edits, small distribution mismatches compound across turns and reduce stability—this effect is exacerbated when the model can attend only to a short slice of the history.

This phenomenon suggests that naively applying single-turn edit models to multi-turn editing will amplify exposure bias and lead to rapid failure. To mitigate this, multi-turn training and inference strategies should be considered, for example: training with model-generated rollouts (teacher-student or scheduled sampling) to reduce distribution mismatch, or increasing the history window / using full-history conditioning when feasible.

In summary, autoregressive/full-history architectures exhibit greater stability in multi-turn editing, whereas short-window non-AR models—especially those trained for single-turn flow matching—are more vulnerable to exposure bias. Future work should evaluate the mitigation strategies above and quantify their impact on multi-turn robustness.

Marginal Success Rate Across Instruction Types. We analyze marginal subtask success rates across turns for different instruction types. The results for GPT-Image-1 are shown in Fig. 5. Other editing models exhibit similar behavior. GPT-Image-1 performs relatively well on attribute-centric tasks such as `color_alter` and `material_alter`, but poorly on `position_change` and `count_change`, indicating weaknesses in spatial and numerical reasoning, respectively.

Among all subtasks, *count_change* is the most challenging. Even the best-performing model (GPT-Image-1) achieves a success rate below 25% at turn 1, while most models remain under 5%. We also provide illustrative examples in Figure 6. Notably, all non-AR models fail on this prompt.

5.3 CONTENT CONSISTENCY

Beyond successfully implementing editing instructions, multi-turn editing requires attention to *consistency*. We evaluate two aspects: (i) **unchanged-object consistency**, which measures whether objects that are not edited up to turn i remain unchanged, and (ii) **background consistency**, which assesses whether the background remains stable when it is not explicitly modified.

We can evaluate consistency in two ways: 1) extract object features with DINOv3 and compute cosine similarity; 2) measure pixel-level consistency using the L_1 distance and report one minus this value. Note that when calculating consistency, the grounding box is extracted from the raw input image and applied to all edited images. We therefore choose to report DINOv3 for consistency

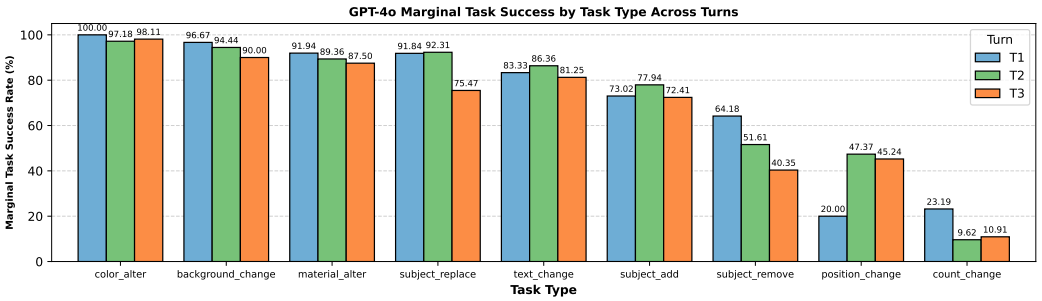

Figure 5: Marginal task success rate grouped by task types for GPT-Image-1. It performs relatively well on attribute-centric tasks such as `color_alter` and `material_alter`, but poorly on `position_change` and `count_change`, indicating weaknesses in spatial and numerical reasoning, respectively. We note that other editing models exhibit similar behavior.

(a) Base Image (b) GPT-Image-1 (✓) (c) Nano Banana (✓) (d) Gemini 2.0 Flash (×) (e) Qwen-Image-Edit (×)

Figure 6: Example of the *count_change* task: changing the number of paper cups to five.

computation because even small shifts in object location can lead to large variations in pixel-wise L_1 loss, even when unchanged objects are well preserved. By relying on DINO features, we ensure that consistency is measured semantically, capturing attributes such as object identity, attributes, and texture, etc. Nevertheless, the consistency scores from DINOv3 remain highly correlated with those computed using pixel-wise L_1 loss (See results in the Appendix).

Based on the results, the most consistent editing model is **FLUX.1-Kontext-dev**, followed by **Nano Banana**. In contrast, **GPT-Image-1** ranks near the bottom, showing notably poor consistency across turns. Representative qualitative examples are shown in Figure 7 and Figure 8.

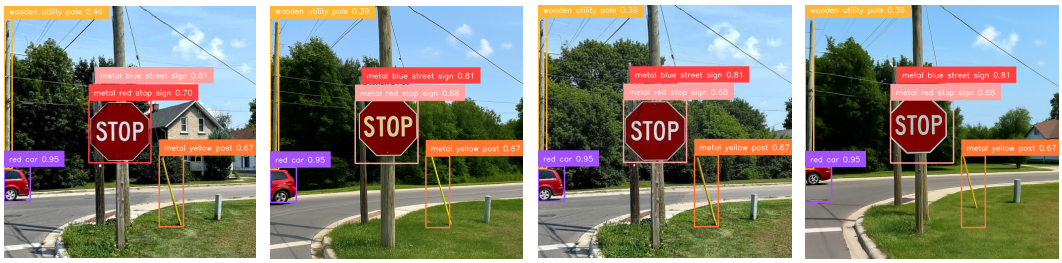

(a) Base Image (b) GPT-Image-1 (95.19) (c) Nano Banana (98.05) (d) Qwen-Image-Edit (94.96)

Figure 7: **Illustration of object consistency.** Instruction: "Remove brick beige house." The grounding box, extracted from the raw input image, highlights the localized region used to compute unchanged-object consistency. The corresponding consistency score is shown in brackets.

5.4 Visual Quality

Beyond instruction following and content consistency, the perceptual *quality* of the edited image is a key dimension. We therefore report (i) a learned aesthetic score and (ii) several low-level image statistics that can surface systematic artifacts and drift in multi-turn editing pipelines.

5.4.1 Aesthetics

We quantify aesthetics with **HPSv3** Ma et al. (2025a), which we found to generalize reliably to our generated images, whereas alternatives (e.g., RAHF Liang et al. (2024)) underperform in this setting. We *do not* fold these quality metrics into the aggregate "Overall" score, as preferences differ on whether an edited image should strictly preserve the input style or pursue beautification.

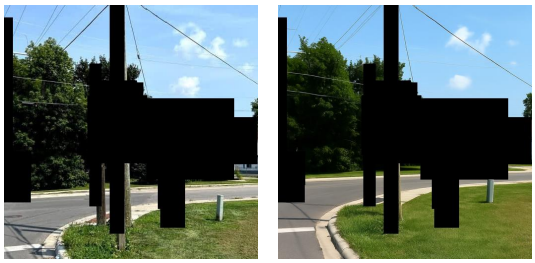

(a) Base Image (b) Qwen-Image-Edit

Figure 8: **Illustration of background consistency.** Instruction: "Remove brick beige house." The grounding box is derived from the union of the raw and edited images, **excluding** the removed object region. This box is used to compute background consistency.

To disentangle these preferences, we report the absolute change in aesthetic score relative to the base image: $\Delta_i = \left|\mathrm{HPS}_{\mathrm{turn}\,i} - \mathrm{HPS}_{\mathrm{base}}\right|$. Smaller Δ indicates stronger style fidelity to the base image; larger Δ reflects greater beautification or stylistic drift. As summarized in Table 3, **GPT-Image-1** achieves the highest aesthetic scores across turns and remains stable. **Qwen-Image-Edit** is the next strongest on absolute HPS. For preserving the base image's look (small Δ), **Gemini 2.0 Flash** shows the least drift, with **Nano Banana** also performing well.

Table 3: Human Preference Scores (HPS), absolute change Δ, and techniques across three refinement turns. dark red denotes the *best* value in the column (i.e., the least difference in human preference score); lighter red denotes the *second-best*. For the HPS columns higher values are better (stronger perceived aesthetics). For the Δ columns smaller values are better (stronger fidelity to the base image).

Technique	Model	Human Preference Score			Δ		
		T1	T2	T3	T1	T2	T3
Autoregressive	Nano Banana	4.94	5.12	5.26	0.56	0.73	0.88
	GPT-Image-1	6.65	6.59	6.56	2.27	2.21	2.18
	Gemini 2.0 Flash	4.44	4.23	4.07	0.05	0.15	0.32
Flow Matching	Qwen-Image-Edit	5.86	5.72	5.15	1.47	1.34	0.77
	Step1X-Edit	4.06	3.34	2.76	0.33	1.04	1.63
	FLUX.1-Kontext-dev	5.12	5.07	5.04	0.73	0.69	0.65
	OmniGen	4.61	4.07	3.50	0.23	0.31	0.89
Diffusion	AnyEdit	3.66	2.80	1.95	0.72	1.58	2.44
	UltraEdit	4.79	4.68	4.36	0.41	0.30	0.02
	MagicBrush	3.85	3.08	2.36	0.54	1.30	2.02
	IP2P	3.20	2.38	1.44	1.18	2.01	2.94

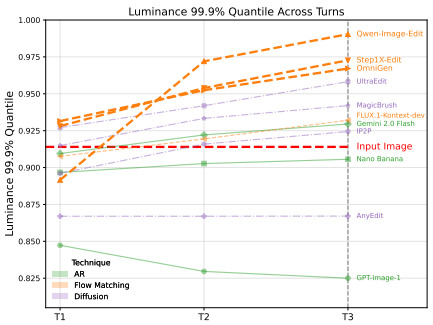

Figure 9: Per-image 99.9% luminance quantile across turns. Higher values indicate more extreme bright pixels and greater risk of over-exposure.

5.4.2 Low-level image statistics

In addition to learned aesthetic scores, we compute several low-level image statistics that help reveal systematic, multi-turn editing artifacts. Concretely, we convert RGB pixels to luminance using the Rec. 709 luma coefficients: $Y = 0.2126\,R + 0.7152\,G + 0.0722\,B$, and for each edited image we extract the **99.9% luminance quantile** (the per-image pixel value below which 99.9% of pixels fall). The 99.9% quantile is sensitive to high-exposure pixels and therefore highlights over-exposure and bright streaks while being robust to single-pixel outliers. In Figure 9 we plot the trend of this statistic across turns.

The measured trend shows a clear pattern: **Qwen-Image-Edit** and several other flow-matching models (with the notable exception of **FLUX.1-Kontext-dev**) exhibit a pronounced increase in the 99.9% luminance quantile over turns, indicating progressive brightening and increased risk of over-exposure. By contrast, regeneration-style editors such as **GPT-Image-1** tend to produce lower luminance values than the input (reflecting darker, more conservative reconstructions), and several models remain stable across turns.

Figure 10 provides qualitative examples from Qwen-Image-Edit. The edited images exhibit elevated luminance and noticeable high-frequency bright artifacts (e.g., white streaks or "line" textures) that degrade perceptual quality, with luminance quintiles increasing substantially. Correspondingly, HPS

drops from 6.19 to 4.19 and 3.34, suggesting that HPS is sensitive to over-exposure to some extent. In contrast, when querying VLMs about the visual quality of these images, the returned scores do not change in the first two turns and remain consistently above 50, reflecting a *positive* evaluation under the [0, 100] scale, while the T2/T3 edited images show significant artifacts.

(a) HPS: 4.25
VLM: 85
Luminance:0.7

(b) HPS: 6.19
VLM: 85
Luminance: 0.60

(c) HPS: 4.19
VLM: 85
Luminance: 0.97

(d) HPS: 3.34
VLM: 60
Luminance: 1.00

Figure 10: Representative Qwen-Image-Edit examples illustrating over-exposure and bright artifact formation across turns. Although editing instructions are often satisfied, the images show elevated luminance and high-frequency bright streaks that accompany the edits (visible especially in T2/T3). Editing instructions: [Remove polyester white skirt, Change the count of tennis ball to 4, Change the color of tank top to blue]. Note that VLM gives a *positive* score to all the images.

5.5 Multi-turn editing vs. complex editing

We compare two strategies for applying multiple edits. In *multi-turn* editing, instructions are executed sequentially: apply instruction 1, then apply instruction 2 to the result, and so on. In *complex* editing, we concatenate C instructions into a single prompt and perform one edit ("complex level C, $C \in \{1, 2, 3\}$"). We evaluate two metrics: (i) the Turn-3 *instruction-following* rate (all edits up to turn 3 succeed), and (ii) the *marginal success* of the final instruction in a C-instruction complex prompt.

Empirically (Table 4; Figure 11), flow-matching editors (short-history condition) behave differently from AR editors when comparing multi-turn and complex modes. AR models tend to achieve higher final-task success in the multi-turn setting, demonstrating the benefit of a step-by-step "chain of edits" (analogous to chain-of-thought for reasoning). By contrast, many flow-matching models obtain better final-task performance under complex (single-shot) editing: sequential edits amplify failure modes (most notably exposure-related drift), which degrades multi-turn performance.

Figure 11 shows that marginal success for the final instruction remains largely stable as complex prompt length increases. Together with the multi-turn drops seen in Figure 4, this pattern supports an *exposure-bias* explanation: performance degradation primarily stems from error accumulation across sequential edits rather than an intrinsic inability to handle multiple instructions in a single prompt.

Practical recommendation: For true step-by-step workflows, we recommend using autoregressive architectures. For flow-matching editors, it is preferable to either (i) pack multiple edits into a single complex prompt when the instruction sequence is known in advance, or (ii) increase the model's history window and/or add inter-turn regularization (e.g., histogram matching, exposure penalties, or periodic reconstruction passes) to mitigate cumulative drift.

6 Limitation and Discussion

Given the object-centric evaluations conducted in this study, several limitations warrant consideration. First, our instruction types are limited to object-centric prompts, which may not capture the full range of creative editing requests typical in real-world scenarios. Future research should explore a broader spectrum of instructions, including those involving stylistic changes or complex narrative elements.

Table 4: Turn-3 instruction following: Multi-turn vs. single-shot complex prompts, grouped by technique. **Bold** indicates which setting is higher for each model.

Technique	Model	Multi-turn (T3)	Complex (C3)
Autoregressive	Nano Banana	**35.35**	28.14
	GPT-Image-1	**38.35**	28.78
	Gemini 2.0 Flash	**28.42**	21.89
Flow Matching	Qwen-Image-Edit	22.55	**27.62**
	Step1X-Edit	**17.83**	15.73
	FLUX.1-Kontext-dev	16.61	**19.58**
	OmniGen	10.66	**11.01**
Diffusion	AnyEdit	7.22	2.80
	UltraEdit	6.36	8.22
	MagicBrush	4.90	4.55
	IP2P	2.80	2.80

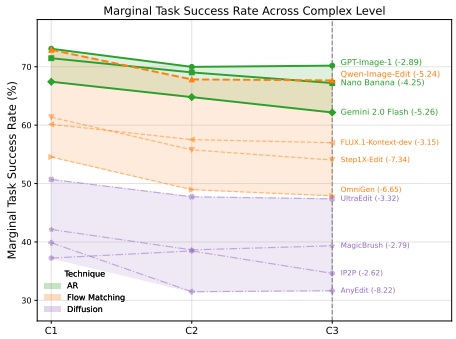

Figure 11: Marginal task-success rate of the *last* instruction as a function of complex prompt length (levels $C = 1, 2, 3$).

Additionally, while our work provides a reliable and comprehensive evaluation framework for multi-turn editing, it does not apply the evaluation results to improve the editing models themselves. A straightforward extension would be to use evaluation scores for Best-of-N selection to improve inference-time performance. Future work could also explore post-training methods such as reinforcement learning, treating the evaluation scores as reward signals.

7 Conclusion

We introduced **EdiVal-Agent**, a scalable, automated, and interpretable framework for evaluating instruction-based image editing. By leveraging symbolic object decomposition, structured instruction generation, and a hybrid evaluation pipeline integrating both specialist tools and vision-language reasoning models, **EdiVal-Agent** enables fine-grained, object-centric assessment of modern editing systems. Our design emphasizes transparency, extensibility, and real-world applicability—providing a new standard for evaluating multi-turn, compositional visual editing. We hope **EdiVal-Agent** will serve as a valuable resource for benchmarking, diagnosing, and advancing the next generation of instruction-based editing models.

References

Shuai Bai, Keqin Chen, Xuejing Liu, Jialin Wang, Wenbin Ge, Sibo Song, Kai Dang, Peng Wang, Shijie Wang, Jun Tang, et al. Qwen2. 5-vl technical report. *arXiv preprint arXiv:2502.13923*, 2025.

Zechen Bai, Pichao Wang, Tianjun Xiao, Tong He, Zongbo Han, Zheng Zhang, and Mike Zheng Shou. Hallucination of multimodal large language models: A survey. *arXiv preprint arXiv:2404.18930*, 2024.

Tim Brooks, Aleksander Holynski, and Alexei A Efros. Instructpix2pix: Learning to follow image editing instructions. In *Proceedings of the IEEE/CVF conference on computer vision and pattern recognition*, pp. 18392–18402, 2023.

Mathilde Caron, Hugo Touvron, Ishan Misra, Hervé Jégou, Julien Mairal, Piotr Bojanowski, and Armand Joulin. Emerging properties in self-supervised vision transformers. In *Proceedings of the International Conference on Computer Vision (ICCV)*, 2021.

Yingshan Chang, Yasi Zhang, Zhiyuan Fang, Ying Nian Wu, Yonatan Bisk, and Feng Gao. Skews in the phenomenon space hinder generalization in text-to-image generation. In Aleš Leonardis, Elisa Ricci, Stefan Roth, Olga Russakovsky, Torsten Sattler, and Gül Varol (eds.), *Computer Vision – ECCV 2024*, pp. 422–439, Cham, 2025. Springer Nature Switzerland. ISBN 978-3-031-73021-4.

Boyuan Chen, Zhuo Xu, Sean Kirmani, Brain Ichter, Dorsa Sadigh, Leonidas Guibas, and Fei Xia. Spatialvlm: Endowing vision-language models with spatial reasoning capabilities. In *Proceedings*

of the IEEE/CVF Conference on Computer Vision and Pattern Recognition, pp. 14455–14465, 2024.

An-Chieh Cheng, Hongxu Yin, Yang Fu, Qiushan Guo, Ruihan Yang, Jan Kautz, Xiaolong Wang, and Sifei Liu. Spatialrgpt: Grounded spatial reasoning in vision-language models. *Advances in Neural Information Processing Systems*, 37:135062–135093, 2024.

Google Deepmind. Gemini 2.5: Pushing the frontier with advanced reasoning, multimodality, long context, and next generation agentic capabilities, 2025. URL https://arxiv.org/abs/2507.06261.

Rinon Gal, Or Patashnik, Haggai Maron, Amit H Bermano, Gal Chechik, and Daniel Cohen-Or. Stylegan-nada: Clip-guided domain adaptation of image generators. *ACM Transactions on Graphics (TOG)*, 41(4):1–13, 2022.

Google Gemini2. Experiment with gemini 2.0 flash native image generation. https://developers.googleblog.com/en/experiment-with-gemini-20-flash-native-image-generation/, 2025. Accessed: 2025-06-22.

Dhruba Ghosh, Hannaneh Hajishirzi, and Ludwig Schmidt. Geneval: An object-focused framework for evaluating text-to-image alignment. *Advances in Neural Information Processing Systems*, 36: 52132–52152, 2023.

Amir Hertz, Ron Mokady, Jay Tenenbaum, Kfir Aberman, Yael Pritch, and Daniel Cohen-Or. Prompt-to-prompt image editing with cross-attention control. In *ICLR*, 2023.

Kaiyi Huang, Kaiyue Sun, Enze Xie, Zhenguo Li, and Xihui Liu. T2i-compbench: A comprehensive benchmark for open-world compositional text-to-image generation. *Advances in Neural Information Processing Systems*, 36:78723–78747, 2023.

Mude Hui, Siwei Yang, Bingchen Zhao, Yichun Shi, Heng Wang, Peng Wang, Yuyin Zhou, and Cihang Xie. Hq-edit: A high-quality dataset for instruction-based image editing. *arXiv preprint arXiv:2404.09990*, 2024.

Max Ku, Dongfu Jiang, Cong Wei, Xiang Yue, and Wenhu Chen. Viescore: Towards explainable metrics for conditional image synthesis evaluation. *arXiv preprint arXiv:2312.14867*, 2023.

Black Forest Labs, Stephen Batifol, Andreas Blattmann, Frederic Boesel, Saksham Consul, Cyril Diagne, Tim Dockhorn, Jack English, Zion English, Patrick Esser, Sumith Kulal, Kyle Lacey, Yam Levi, Cheng Li, Dominik Lorenz, Jonas Müller, Dustin Podell, Robin Rombach, Harry Saini, Axel Sauer, and Luke Smith. Flux.1 kontext: Flow matching for in-context image generation and editing in latent space, 2025. URL https://arxiv.org/abs/2506.15742.

Youwei Liang, Junfeng He, Gang Li, Peizhao Li, Arseniy Klimovskiy, Nicholas Carolan, Jiao Sun, Jordi Pont-Tuset, Sarah Young, Feng Yang, Junjie Ke, Krishnamurthy Dj Dvijotham, Katie Collins, Yiwen Luo, Yang Li, Kai J Kohlhoff, Deepak Ramachandran, and Vidhya Navalpakkam. Rich human feedback for text-to-image generation. In *Proceedings of the IEEE/CVF Conference on Computer Vision and Pattern Recognition*, 2024.

Yaron Lipman, Ricky TQ Chen, Heli Ben-Hamu, Maximilian Nickel, and Matt Le. Flow matching for generative modeling. *arXiv preprint arXiv:2210.02747*, 2022.

Shilong Liu, Zhaoyang Zeng, Tianhe Ren, Feng Li, Hao Zhang, Jie Yang, Qing Jiang, Chunyuan Li, Jianwei Yang, Hang Su, et al. Grounding dino: Marrying dino with grounded pre-training for open-set object detection. In *European conference on computer vision*, pp. 38–55. Springer, 2024a.

Shilong Liu, Zhaoyang Zeng, Tianhe Ren, Feng Li, Hao Zhang, Jie Yang, Qing Jiang, Chunyuan Li, Jianwei Yang, Hang Su, et al. Grounding dino: Marrying dino with grounded pre-training for open-set object detection. In *European Conference on Computer Vision*, pp. 38–55. Springer, 2024b.

Shiyu Liu, Yucheng Han, Peng Xing, Fukun Yin, Rui Wang, Wei Cheng, Jiaqi Liao, Yingming Wang, Honghao Fu, Chunrui Han, et al. Step1x-edit: A practical framework for general image editing. *arXiv preprint arXiv:2504.17761*, 2025.

Xingchao Liu, Chengyue Gong, and Qiang Liu. Flow straight and fast: Learning to generate and transfer data with rectified flow. *arXiv preprint arXiv:2209.03003*, 2022.

Yuhang Ma, Xiaoshi Wu, Keqiang Sun, and Hongsheng Li. Hpsv3: Towards wide-spectrum human preference score, 2025a. URL https://arxiv.org/abs/2508.03789.

Yuhang Ma, Xiaoshi Wu, Keqiang Sun, and Hongsheng Li. Hpsv3: Towards wide-spectrum human preference score. *arXiv preprint arXiv:2508.03789*, 2025b.

OpenAI. Introducing 4o image generation. https://openai.com/index/introducing-4o-image-generation/, 2025. Accessed: 2025-06-22.

Dustin Podell, Zion English, Kyle Lacey, Andreas Blattmann, Tim Dockhorn, Jonas Müller, Joe Penna, and Robin Rombach. SDXL: Improving latent diffusion models for high-resolution image synthesis. In *The Twelfth International Conference on Learning Representations*, 2024. URL https://openreview.net/forum?id=di52zR8xgf.

Muhammad Fetrat Qharabagh, Mohammadreza Ghofrani, and Kimon Fountoulakis. Lvlm-count: Enhancing the counting ability of large vision-language models. *arXiv preprint arXiv:2412.00686*, 2024.

Alec Radford, Jong Wook Kim, Chris Hallacy, Aditya Ramesh, Gabriel Goh, Sandhini Agarwal, Girish Sastry, Amanda Askell, Pamela Mishkin, Jack Clark, et al. Learning transferable visual models from natural language supervision. In *International conference on machine learning*, pp. 8748–8763. PmLR, 2021.

Aditya Ramesh, Prafulla Dhariwal, Alex Nichol, Casey Chu, and Mark Chen. Hierarchical text-conditional image generation with clip latents. *arXiv preprint arXiv:2204.06125*, 1(2):3, 2022.

Robin Rombach, Andreas Blattmann, Dominik Lorenz, Patrick Esser, and Björn Ommer. High-resolution image synthesis with latent diffusion models. In *Proceedings of the IEEE/CVF conference on computer vision and pattern recognition*, pp. 10684–10695, 2022.

Shelly Sheynin, Adam Polyak, Uriel Singer, Yuval Kirstain, Amit Zohar, Oron Ashual, Devi Parikh, and Yaniv Taigman. Emu edit: Precise image editing via recognition and generation tasks. In *Proceedings of the IEEE/CVF Conference on Computer Vision and Pattern Recognition*, pp. 8871–8879, 2024.

Oriane Siméoni, Huy V Vo, Maximilian Seitzer, Federico Baldassarre, Maxime Oquab, Cijo Jose, Vasil Khalidov, Marc Szafraniec, Seungeun Yi, Michaël Ramamonjisoa, et al. Dinov3. *arXiv preprint arXiv:2508.10104*, 2025.

An Vo, Khai-Nguyen Nguyen, Mohammad Reza Taesiri, Vy Tuong Dang, Anh Totti Nguyen, and Daeyoung Kim. Vision language models are biased. *arXiv preprint arXiv:2505.23941*, 2025.

Chenfei Wu, Jiahao Li, Jingren Zhou, Junyang Lin, Kaiyuan Gao, Kun Yan, Sheng ming Yin, Shuai Bai, Xiao Xu, Yilei Chen, Yuxiang Chen, Zecheng Tang, Zekai Zhang, Zhengyi Wang, An Yang, Bowen Yu, Chen Cheng, Dayiheng Liu, Deqing Li, Hang Zhang, Hao Meng, Hu Wei, Jingyuan Ni, Kai Chen, Kuan Cao, Liang Peng, Lin Qu, Minggang Wu, Peng Wang, Shuting Yu, Tingkun Wen, Wensen Feng, Xiaoxiao Xu, Yi Wang, Yichang Zhang, Yongqiang Zhu, Yujia Wu, Yuxuan Cai, and Zenan Liu. Qwen-image technical report, 2025a. URL https://arxiv.org/abs/2508.02324.

Chenyuan Wu, Pengfei Zheng, Ruiran Yan, Shitao Xiao, Xin Luo, Yueze Wang, Wanli Li, Xiyan Jiang, Yexin Liu, Junjie Zhou, Ze Liu, Ziyi Xia, Chaofan Li, Haoge Deng, Jiahao Wang, Kun Luo, Bo Zhang, Defu Lian, Xinlong Wang, Zhongyuan Wang, Tiejun Huang, and Zheng Liu. Omnigen2: Exploration to advanced multimodal generation. *arXiv preprint arXiv:2506.18871*, 2025b.

Shitao Xiao, Yueze Wang, Junjie Zhou, Huaying Yuan, Xingrun Xing, Ruiran Yan, Chaofan Li, Shuting Wang, Tiejun Huang, and Zheng Liu. Omnigen: Unified image generation. In *Proceedings of the Computer Vision and Pattern Recognition Conference*, pp. 13294–13304, 2025.

Jiazheng Xu, Xiao Liu, Yuchen Wu, Yuxuan Tong, Qinkai Li, Ming Ding, Jie Tang, and Yuxiao Dong. Imagereward: learning and evaluating human preferences for text-to-image generation. In *Proceedings of the 37th International Conference on Neural Information Processing Systems*, pp. 15903–15935, 2023.

An Yang, Baosong Yang, Beichen Zhang, Binyuan Hui, Bo Zheng, Bowen Yu, Chengyuan Li, Dayiheng Liu, Fei Huang, Haoran Wei, Huan Lin, Jian Yang, Jianhong Tu, Jianwei Zhang, Jianxin Yang, Jiaxi Yang, Jingren Zhou, Junyang Lin, Kai Dang, Keming Lu, Keqin Bao, Kexin Yang, Le Yu, Mei Li, Mingfeng Xue, Pei Zhang, Qin Zhu, Rui Men, Runji Lin, Tianhao Li, Tingyu Xia, Xingzhang Ren, Xuancheng Ren, Yang Fan, Yang Su, Yichang Zhang, Yu Wan, Yuqiong Liu, Zeyu Cui, Zhenru Zhang, and Zihan Qiu. Qwen2.5 technical report. *arXiv preprint arXiv:2412.15115*, 2024.

Siwei Yang, Mude Hui, Bingchen Zhao, Yuyin Zhou, Nataniel Ruiz, and Cihang Xie. Complex-edit: Cot-like instruction generation for complexity-controllable image editing benchmark. *arXiv preprint arXiv:2504.13143*, 2025.

Qifan Yu, Wei Chow, Zhongqi Yue, Kaihang Pan, Yang Wu, Xiaoyang Wan, Juncheng Li, Siliang Tang, Hanwang Zhang, and Yueting Zhuang. Anyedit: Mastering unified high-quality image editing for any idea. In *Proceedings of the Computer Vision and Pattern Recognition Conference*, pp. 26125–26135, 2025.

Kai Zhang, Lingbo Mo, Wenhu Chen, Huan Sun, and Yu Su. Magicbrush: A manually annotated dataset for instruction-guided image editing. *Advances in Neural Information Processing Systems*, 36:31428–31449, 2023.

Yasi Zhang, Peiyu Yu, Yaxuan Zhu, Yingshan Chang, Feng Gao, Ying Nian Wu, and Oscar Leong. Flow priors for linear inverse problems via iterative corrupted trajectory matching. In *The Thirty-eighth Annual Conference on Neural Information Processing Systems*, 2024. URL https://openreview.net/forum?id=1H2e7USI09.

Yasi Zhang, Peiyu Yu, and Ying Nian Wu. Object-conditioned energy-based attention map alignment in text-to-image diffusion models. In Aleš Leonardis, Elisa Ricci, Stefan Roth, Olga Russakovsky, Torsten Sattler, and Gül Varol (eds.), *Computer Vision – ECCV 2024*, pp. 55–71, Cham, 2025a. Springer Nature Switzerland. ISBN 978-3-031-72946-1.

Zheyuan Zhang, Fengyuan Hu, Jayjun Lee, Freda Shi, Parisa Kordjamshidi, Joyce Chai, and Ziqiao Ma. Do vision-language models represent space and how? evaluating spatial frame of reference under ambiguities. In *The Thirteenth International Conference on Learning Representations*, 2025b. URL https://openreview.net/forum?id=84pDoCD4lH.

Haozhe Zhao, Xiaojian Shawn Ma, Liang Chen, Shuzheng Si, Rujie Wu, Kaikai An, Peiyu Yu, Minjia Zhang, Qing Li, and Baobao Chang. Ultraedit: Instruction-based fine-grained image editing at scale. *Advances in Neural Information Processing Systems*, 37:3058–3093, 2024.

Algorithm 1 Object Listing and Grounding Filter

Require: image I
Ensure: object pool $\mathcal{O}$ with grounding metadata
$J \leftarrow \textsc{ListObjects}(I)$ ▷ see Sec. A.2.1
$\mathcal{O} \leftarrow \emptyset$
for all (name, attrs) $\in J$ excluding key `All Objects` **do**
  (boxes, phrases, scores) $\leftarrow \textsc{Ground}(I, \text{name})$ ▷ thresholds 0.3–0.4
  if boxes $\neq \emptyset$ **and** each box has $w, h < 0.9$ **and** area ≤ 0.4 **then**
    $\mathcal{O}$[name] $\leftarrow$ attrs; attach grounding metadata (count, boxes, phrases, scores)
  end if
end for
$\mathcal{O}$[`Filtered All Objects`] $\leftarrow \textsc{Join}(\textsc{Keys}(\mathcal{O}), ". ")$ and then append "."

A Algorithmic Details

This appendix provides the algorithmic details of our pipeline: object discovery and grounding-based filtering (decomposition), instruction generation for multi-turn editing, and evaluation (instruction following, consistency, and perceptual quality). We also list the exact prompts and implementation specifics needed for reproducibility, and summarize the model-generation configurations.

A.1 Decomposition

We first enumerate visible objects in an input image using a vision-language model (VLM) prompt, then filter these objects via visual grounding.

- Object listing: We use `GPT-4o` with the prompt in Section A.2.1. The model returns a JSON with one entry per object and a terminal aggregated string key ``` ``All Objects'' ```.
- Grounding filter: We use GroundingDINO SwinT-OGC Liu et al. (2024a) to retain only objects that can be visually grounded. We resize images to 512×512. We keep detections meeting text/box thresholds (0.35) and reject oversized boxes by checking width/height in normalized coordinates; we use `max_box_size=0.9` and filter large regions if area > 0.4. The output augments each kept object with grounding counts, phrases, boxes, and scores, and creates a ``` ``Filtered All Objects'' ``` string listing retained objects.

A.2 Instruction Generation

We generate multi-turn editing instructions from the grounded object pool. We support nine task types: local edits {`subject_replace`, `subject_remove`, `material_alter`, `color_alter`, `subject_add`, `text_change`, `position_change`, `count_change`} and the global edit {`background_change`}. We set `MAX_TURNS=3`. At each turn, we sample a new task type without repetition where feasible. Feasibility is checked against the current object pool (e.g., `position_change` requires at least two objects). If a sampled task is infeasible, we fall back to `subject_add`. We maintain an available-objects pool that is updated after each instruction according to its semantics (adds, removes, or modifies attributes). If a background change occurs, we mark `bg_consistency=false` for subsequent turns and restrict the pool to foreground objects for the remainder of the episode.

Prompts (Full Text) Below we reproduce the prompts used by our generators, reformatted for readability in print (content preserved).

A.2.1 Object Listing Prompt

> You will be given an image. Your task is to identify and describe all clearly visible objects in the image in a structured JSON format.
>
> **Output rules:**

Algorithm 2 Multi-Turn Instruction Generation

Require: grounded pool $\mathcal{O}_0$, turns T=3
Ensure: tasks $\{\tau_t\}$, instructions $\{I_t\}$, formats $\{F_t\}$, flag has_bg, set all_objects_ever
used $\leftarrow \emptyset$; $\mathcal{O} \leftarrow \mathcal{O}_0$; has_bg $\leftarrow$ false
all_edited $\leftarrow \emptyset$; all_objects_ever $\leftarrow$ keys($\mathcal{O}_0$)
for $t = 1$ to T **do**
    cand $\leftarrow$ {all task types} $\setminus$ used
    $\tau_t \leftarrow$ sample(cand);
    if not feasible($\tau_t, \mathcal{O}$) **then** $\tau_t \leftarrow$ `subject_add`
    end if
    $F_t \leftarrow$ format_instruction($\tau_t, \mathcal{O}$) ▷ Query VLM by prompts in Section A.2.2
    $I_t \leftarrow$ render_instruction($F_t, \tau_t, \mathcal{O}$) ▷ strip brackets; add unchanged list for background
    used $\leftarrow$ used $\cup \{\tau_t\}$; append F_t, I_t
    Update *all_object_pool* by adding any objects introduced in instruction I_t.
    Update *available_object_pool* by adding or removing objects as specified in I_t.
    Update *unchanged_objects_pool* by removing any objects affected by I_t.
    if $\tau_t =$ `background_change` **then**
        has_bg $\leftarrow$ true; $\mathcal{O} \leftarrow$ filter_foreground($\mathcal{O}$)
    end if
end for
return $\{\tau_t\}, \{I_t\}, \{F_t\}$, has_bg, all_objects_ever

1. Each object must be listed as a key in the JSON, using the format: "{material} {color} {object name}". If the material or color is unknown, omit that part. Do not include any visible text in the key. Do not use "person" as an object name; instead, describe wearable items (e.g., "blue cotton shirt").
2. For each object, the value is a dictionary with fields: "object" (type, e.g., shirt, cup), "color" (dominant color, use null if unknown), "material" (likely material, use null if unknown), "text" (visible text, null if none), "count" (number of instances), and "foreground" (boolean).
3. Do not include objects that are too small to describe, mostly occluded/incomplete, or only background scenery (e.g., distant sky, wall, floor).
4. Add a final key "All Objects" whose value is a single string listing all object names, formatted as: "{material} {color} {object name}. {color} {object name}. {material} {object name}. {object name}." Exclude "null"/"None" and separate entries by ". " (period + space). Do not include any text content in this list.

Example output (abridged JSON):

- "cotton blue shirt": {object: "shirt", color: "blue", material: "cotton", text: null, count: 1, foreground: true}
- "ceramic white cup": {object: "cup", color: "white", material: "ceramic", text: "GOOD DAY", count: 1, foreground: false}
- "leather bag": {object: "bag", color: null, material: "leather", text: null, count: 2, foreground: true}
- "red scarf": {object: "scarf", color: "red", material: null, text: null, count: 1, foreground: true}
- "All Objects": "cotton blue shirt. ceramic white cup. leather bag. red scarf."

A.2.2 Task Prompts

Subject Replace

You are given an image and asked to suggest a replacement object for a specific object in the scene.

Given object to replace: *object_name*

Your task:

1. Understand the scene context.
2. Suggest a new object that naturally replaces "*object_name*".

3. Ensure the suggestion is realistic for the scene.
4. Respond with only the object name (e.g., “chair”, “lamp”, “book”).

Examples: In a kitchen: “bowl”, “mug”; on a street: “bus”, “truck”; in an office: “stool”, “bench”.

Answer format: New object name:

Material Alter

You are given an image and asked to suggest a new material for a specific object.

Object: *object_name* **Current material:** *current_material*

Your task:

1. Identify the object.
2. Suggest a realistic alternative material that is easy to distinguish from the current one.
3. Respond with only the material name (e.g., “wood”, “metal”, “plastic”, “leather”).

Examples: cup: ceramic, glass, metal, plastic; chair: wood, metal, plastic, fabric; bag: leather, canvas, nylon, fabric.

Answer format: New material:

Position Change

You are given an image and asked to create a position change instruction.

Available objects: *available objects* **Positions:** left, right, above, below

Your task:

1. Select a target object to move and a reference object.
2. Choose a relative position (left, right, above, below).
3. Ensure the instruction is physically reasonable.
4. **Format:** “Change the position of [target object] to [position] of [reference object]”.

Examples: “Change the position of [cup] to [right] of [book]”; “Change the position of [lamp] to [above] of [table]”.

Answer format: Position change instruction:

Count Change

You are given an image and asked to create a count change instruction.

Available objects: *available objects* **Target count:** *target count*

Your task:

1. Identify a suitable object for the requested count.
2. Ensure the target count is realistic for the scene.
3. **Format:** “Change the count of [object name] to [target count]”.

Examples: “Change the count of [cup] to [3]”; “Change the count of [book] to [2]”.

Answer format: Count change instruction:

Text Change

You are given an image and asked to generate new text content.

Context: *text situation*

Your task:

1. Generate text that fits the scene.
2. Keep text short: *max 2 words in English or 4 Chinese characters*.
3. Respond with only the text content (no quotes or extra words).

Examples: coffee shop: “COFFEE”, “OPEN”; book: “NOVEL”, “GUIDE”; sign: “EXIT”, “STOP”; Chinese: “ 咖啡 ”, “ 出口 ”.

Answer format: New text:

Color Alter

You are given an image and asked to suggest a new color for a specific object.
Object: *object name* **Current color:** *current color*
Your task:

1. Suggest a simple, common color that fits the object.
2. Use only basic colors: red, blue, green, yellow, black, white, brown, gray, orange, purple, pink.
3. Choose a color different from the current color and answer with the color name only.

Answer format: New color:

Subject Add

You are given an image and asked to suggest a new object to add to the scene.
Reference object: *reference object* **Position:** *position*
Your task:

1. Propose an object that would naturally fit at the specified position relative to the reference object.
2. Ensure the suggestion is realistic and contextually appropriate.
3. Respond with only the object name (e.g., "lamp", "book", "cup").

Examples: next to a desk: "chair", "lamp", "computer"; near a kitchen counter: "bowl", "plate", "mug"; by a window: "plant", "curtain", "book".
Answer format: New object:

Background Change

You are given an image and asked to suggest a new background for the scene. The existing objects should remain unchanged.
Your task:

1. Propose a new background that works with the current setting.
2. Keep it simple and realistic; use 1–2 words (e.g., "kitchen", "office", "garden", "beach", "forest").
3. Respond with only the background name.

Answer format: New background:

A.3 EVALUATION

We evaluate in two modes: (i) **Multi-turn** (each turn edits the output of the previous turn), and (ii) **Complex Editing** (compress all instructions to a single prompt).

Instruction Following. We compute a binary success per instruction with a detector combining GroundingDINO Liu et al. (2024a) and a VLM (Qwen2-VL-7B) Bai et al. (2025). Representative details:

- Detector thresholds. Unless noted per task, GroundingDINO thresholds are 0.3–0.4; detections return normalized boxes $[x_1, y_1, x_2, y_2]$.
- Cropping and small objects. For object-level checks we crop by detected boxes; very small boxes (<0.05 in width/height) can be enlarged before VLM queries.
- Replace. Detect old and new objects in source/target; success if both are detected and any IoU between a source box (old) and a target box (new) is > 0. A VLM pre-check rejects obvious non-replacements. See details in Alg 3.
- Remove. Detect the object in the source; success if the object is absent in the target. See details in Alg 4.
- Position change. Detect target and reference objects and verify the requested spatial relation using object centers; also ensure the object count did not increase spuriously. See details in Alg 6.
- Count change. Use the detector to locate instances of the target object and take the number of validated detections as the count. See details in Alg 7.

Algorithm 3 Evaluate Subject Replace

Require: base B, target T, old object name o, new object name n
Ensure: success flag succ
$S \leftarrow \textsc{Detect}(B, o, \tau)$; $\quad T_n \leftarrow \textsc{Detect}(T, n, \tau)$
if $S \neq \emptyset \ \wedge \ T_n \neq \emptyset$ **then**
    succ $\leftarrow \max_{b \in S,\, t \in T_n} \textsc{IoU}(b, t) > 0$
else
    succ $\leftarrow$ false
end if
return succ

Algorithm 4 Evaluate Subject Remove

Require: base B, target T, object name o
Ensure: success flag succ
$S \leftarrow \textsc{Detect}(B, o, \tau)$; $\quad T_o \leftarrow \textsc{Detect}(T, o, \tau)$
succ $\leftarrow (S \neq \emptyset \wedge T_o = \emptyset)$
return succ

- Color/material. Crop the object in the target and ask the VLM a yes/no question about the new color/material. See details in Alg 8 and Alg 9.
- Text change. If the instruction adds text anywhere, run the VLM on the whole image; if it replaces text on a specific object, first crop that object's box, ask the VLM to extract the text, and compare it to the requested text. See details in Alg 10.
- Background change. Ask the VLM yes/no whether the requested background category is present. See details in Alg 11.

Consistency. We measure object and background stability as follows:

- Object consistency (unchanged objects): DINOv3 ViT-B/16 Siméoni et al. (2025) feature similarity between crops of unchanged objects in base vs. target; we also report pixel L1 consistency and average across objects per image.
- Background consistency: detect objects in all_objects_pool in base/target (GroundingDINO), mask them to isolate background, then compute masked L1 between backgrounds (optionally DINOv3 masked similarity). Background consistency is evaluated only when no background change occurred earlier (`bg_consistency=true`).

Perceptual Quality. We report HPSv3 Ma et al. (2025a) plausibility and aesthetics, plus luminance metrics. Quality is *not* folded into the *Overall* score.

A.4 Overall Score and Aggregation Details

Let α_t be the image success rate at turn t: the fraction of images for which *all* edits up to and including turn t are successful (aggregated per task type, then averaged). Let κ denote the average content-consistency score combining object and background DINOv3 similarities when applicable.

- Overall score. We report

$$\text{Overall} = \left[\text{mean}_t(\alpha_t) \ \times \ \text{mean}(\kappa)\right]^{1/2}.$$

- Missing outputs across turns. For summary tables, we include only images that produce all required outputs for the evaluated mode. If a model fails to generate a later turn, that image is omitted from later-turn aggregates for that mode. Some edits will be rejected by some models since the sensitive content flag.
- No unchanged objects. If the unchanged-object list is empty, object consistency is recorded as `None` and excluded from averages; background consistency is still computed when `bg_consistency=true`.

Algorithm 5 Evaluate Subject Add

Require: base B, target T, new object name n, optional reference object name r, optional position $p \in \{\text{left}, \text{right}, \text{above}, \text{below}\}$
Ensure: success flag
$B_n \leftarrow \textsc{Detect}(B, n, \tau)$; $T_n \leftarrow \textsc{Detect}(T, n, \tau)$
if $T_n = \emptyset \ \vee \ B_n \neq \emptyset$ **then**
  return false
end if
if r and p are provided **then**
  $B_r \leftarrow \textsc{Detect}(B, r, \tau)$; $T_r \leftarrow \textsc{Detect}(T, r, \tau)$
  if $T_r = \emptyset$ **then**
    return false
  end if
  Choose max logits boxes $t \in T_n$, $u \in T_r$
  $(x_t, y_t) \leftarrow \textsc{Center}(t)$; $(x_u, y_u) \leftarrow \textsc{Center}(u)$
  if $p = \text{left} \wedge x_t < x_u - \varepsilon_x$ **then**
    return true
  end if
  if $p = \text{right} \wedge x_t > x_u + \varepsilon_x$ **then**
    return true
  end if
  if $p = \text{above} \wedge y_t < y_u - \varepsilon_y$ **then**
    return true
  end if
  if $p = \text{below} \wedge y_t > y_u + \varepsilon_y$ **then**
    return true
  end if
  return false
else
  return true
end if

- Turn-level reporting. We also report per-turn (`T1`, `T2`, `T3`) instruction-following and consistency, and per-task-type success rates $\alpha_{t,\text{type}}$. Quality metrics are reported separately and are not folded into *Overall*.

A.5 Model generations

We evaluate a mix of closed- and open-source editors using each model's default settings (no hyperparameter tuning):

- GPT-Image-1, Nano Banana, and Gemini 2.0 Flash: called via their APIs with default parameters.
- QWEN Image Edit: default settings from `https://huggingface.co/Qwen/Qwen-Image-Edit`.
- InstructPix2Pix (IP2P): settings from `https://github.com/timothybrooks/instruct-pix2pix`.
- Magicbrush: same settings as IP2P; model weights from `https://huggingface.co/vinesmsuic/magicbrush-jul7`.
- UltraEdit: settings from `https://github.com/HaozheZhao/UltraEdit`; we apply a black mask since no explicit mask is provided.
- AnyEdit: repository at `https://github.com/weichow23/AnySD/tree/9e7d36ef88e237b527695efc90b1abc18fa51218` with `edit_type` set to `general`.
- Step1X-Edit: repository at `https://github.com/stepfun-ai/Step1X-Edit`; weights at `https://huggingface.co/stepfun-ai/Step1X-Edit`.

Algorithm 6 Evaluate Position Change

Require: base B, target T, target object name a, reference object r, position p
Ensure: success flag
$B_a \leftarrow \textsc{Detect}(B, a, \tau)$; $T_a \leftarrow \textsc{Detect}(T, a, \tau)$
$B_r \leftarrow \textsc{Detect}(B, r, \tau)$; $T_r \leftarrow \textsc{Detect}(T, r, \tau)$
if $T_a = \emptyset \ \vee \ T_r = \emptyset$ **then**
  return false
end if
if $|T_a| > |B_a|$ **then**
  return false ▷ No count inflation
end if
Select max logits boxes $t \in T_a$, $u \in T_r$
$(x_t, y_t) \leftarrow \textsc{Center}(t)$; $(x_u, y_u) \leftarrow \textsc{Center}(u)$
if $p =$ left **then**
  return $x_t < x_u - \varepsilon_x$
end if
if $p =$ right **then**
  return $x_t > x_u + \varepsilon_x$
end if
if $p =$ above **then**
  return $y_t < y_u - \varepsilon_y$
end if
if $p =$ below **then**
  return $y_t > y_u + \varepsilon_y$
end if
return false

Algorithm 7 Evaluate Count Change

Require: target T, name o, requested count c^*
Ensure: success flag
$\hat{c} \leftarrow |\textsc{Detect}(T, o)|$
return $(\hat{c} = c^*)$

- OmniGen: repository at `https://github.com/VectorSpaceLab/OmniGen`.
- FLUX: default settings from `https://huggingface.co/black-forest-labs/FLUX.1-Kontext-dev`.

Modes. For clarity in the paper: we report both **Multipass** and **Complex Editing** (renamed from *singlepass* for consistency with the rest of the paper).

Reproducibility Notes. Prompts are provided in full (Section A.2); thresholds are specified above. Grounding uses SwinT-OGC weights; consistency uses DINOv3 ViT-B/16; the quality head follows our RAHF implementation, and HPSv3 is included when available. All other parameters are left at defaults.

B Additional Evaluation Results

In this section, we provide extended evaluation results. We separate the analysis into two modes: *multi-turn editing* and *complex editing*. Each mode is evaluated across three aspects: instruction following, consistency, and quality.

For the multi-turn editing mode, the overall instruction-following success rate is reported in Table 5, while success rates for individual instruction types appear in Tables 6 and 7. Consistency results are summarized in Table 11. We also observed that some input images are non-square after resizing, which can leave black padding on the top/bottom or left/right edges. Certain editing models, such

Algorithm 8 Evaluate Color Alter

Require: target image T, object name o, color k
1: **return** VLMYESNO(T, "Is the o k?")

Algorithm 9 Evaluate Material Alter

Require: target image T, object name o, material m
Ensure: success flag
1: **return** VLMYESNO(T, "Is the o made of m?")

as GPT-Image-1 and Qwen-Image-Edit, attempt to fill these areas, whereas others preserve them. To account for this, we separately report consistency for square (Table 12) and non-square inputs (Table 13). The conclusions remain consistent with the overall evaluation. Quality results for multi-turn editing are presented in Table 15.

For the complex editing mode, the overall instruction-following success rate is shown in Table 8, and per-instruction-type results are in Tables 9 and 10. Consistency and quality results are reported in Tables 14 and 16, respectively.

In consistency table, p99 means 99% quantile of luminance value, and p999 means 99.9% quantile of luminance value.

C HUMAN AGREEMENT

The human study was conducted online through Gradio[3]. Annotators were asked to answer a 2-way multiple-choice problem (Yes/No) about an editing instruction, an original image, and an edited image. There were very limited potential participant risks, if they were to be exposed to an image that was disturbing or not safe for work (NSFW). It is because the source images we used were from GEit-Bench Liu et al. (2025), which were not in themselves offensive. Also, our agent already filtered out unsafe images during the first decomposition stage. Furthermore, all edited images from the models were passed through its own NSFW filters which blacked out any potentially unsafe content.

We conducted human study on edits made by four exemplary models—Step1X-Edit, AnyEdit, Gemini-Flash 2.0, and Flux.1-Kontext-dev—on **EdiVal-Bench**, generated by **EdiVal-Agent** as described in Section A.2. For each edit, we collected two human ratings, yielding a total of $572 \times 4 \times 2 = 4{,}576$ annotations. Depending on the prompt (which affected the editing instruction), each annotation took about 1–2 minutes. Raters were recruited online, each holding at least a bachelor's degree. They were shown the original image, the edited image, and the corresponding instruction, and were asked a binary question: *"Evaluate whether the edited image successfully follows the given instruction."*

D VLMS FAILING TO JUDGE VISUAL QUALITY

The following is the zero-shot prompt for visual quality with VLMs. The example results are shown in Fig. 12.

```
You are an expert at evaluating image visual quality and naturalness.

I will show you an image.

Please analyze whether the image is visually pleasing and natural. Consider:
1. Is the image visually pleasing?
2. Is the image natural?
3. Does the image look natural and coherent?
```

[3] https://www.gradio.app/

Algorithm 10 Evaluate Text Change

Require: target T, desired text t^* (optionally object name)
Ensure: success flag
1: $t \leftarrow \text{VLMTEXT}(T)$
2: Normalize t and t^* (case, punctuation, whitespace)
3: **return** TEXT-MATCH(t, t^*)

Algorithm 11 Evaluate Background Change

Require: target T, category g
Ensure: success flag
1: **return** VLMYESNO$(T,$ "Does the background show g?")

```
Respond only with a score between 0 and 100, where 100 is the highest score.
100 means the image is visually pleasing and natural.
0 means the image is not visually pleasing and natural.
50 means the image is neutral.
```

Table 5: Image success rates and overall task success rates across turns. (Multi-turn model)

Model	Image Success Rate			Overall Task Rate		
	T1	T2	T3	T1	T2	T3
GPT-4o	73.12	54.89	38.35	73.12	74.44	73.12
Nano	70.70	50.66	35.35	70.70	72.59	68.24
Gemini	68.07	45.96	28.42	68.07	67.72	68.42
QWEN	72.90	44.06	22.55	72.90	62.94	56.12
StepEdit	61.89	34.97	17.83	61.89	59.09	53.32
FLUX	59.97	32.69	16.61	59.97	56.29	51.40
OmniGen	54.72	24.48	10.66	54.72	48.60	42.48
AnyEdit	41.07	16.32	7.22	40.03	39.34	40.56
UltraEdit	51.37	17.70	6.36	50.52	36.54	31.47
MagicBrush	42.31	15.73	4.90	42.31	40.73	41.26
IP2P	37.41	10.66	2.80	37.41	32.87	34.27

Table 6: Task success rates (%) across five instruction types and three turns (multi-turn mode).

Model	Subject Replace			Subject Remove			Material Alter			Color Alter			Subject Add		
	T1	T2	T3	T1	T2	T3	T1	T2	T3	T1	T2	T3	T1	T2	T3
GPT-Image-1	84.31	94.64	85.71	70.77	55.93	47.37	96.83	95.65	87.88	100.00	97.06	100.00	80.95	72.46	72.41
Nano Banana	91.84	92.31	75.47	64.18	51.61	40.35	91.94	89.36	87.50	100.00	97.18	98.11	73.02	77.94	72.41
Gemini 2.0 Flash	83.33	92.98	78.18	58.67	53.62	50.82	90.91	82.00	83.33	100.00	89.04	98.21	77.61	72.73	75.27
QWEN-Image-Edit	87.04	82.46	70.91	70.67	31.88	37.70	93.94	90.00	79.17	100.00	97.26	94.74	77.61	55.84	39.78
Step1X-Edit	90.74	96.49	67.27	53.33	30.43	21.31	95.45	80.00	87.50	100.00	100.00	91.23	64.18	57.14	45.16
FLUX.1-Kontext-dev	85.19	80.70	72.73	54.67	42.03	32.79	84.85	74.00	73.61	100.00	98.63	94.74	67.16	61.04	39.78
OmniGen	88.89	84.21	58.18	46.67	21.74	19.67	84.85	72.00	70.83	100.00	90.41	91.23	53.73	51.95	37.63
AnyEdit	74.07	66.67	61.82	37.33	39.13	36.07	78.79	68.00	68.06	78.57	68.49	78.95	22.39	38.96	25.81
UltraEdit	88.89	63.16	38.18	26.67	5.80	6.56	87.88	66.00	63.89	98.21	80.82	78.95	38.81	23.38	9.68
MagicBrush	83.33	75.44	63.64	28.00	18.84	18.03	83.33	86.00	80.56	94.64	87.67	91.23	37.31	41.56	37.63
IP2P	75.93	66.67	65.45	25.33	8.70	18.03	74.24	70.00	65.28	87.50	82.19	75.44	23.88	28.57	19.35

Table 7: Task success rates (%) across four instrcution types and three turns (multi-turn mode).

Model	Text Change			Position Change			Count Change			Background Change		
	T1	T2	T3	T1	T2	T3	T1	T2	T3	T1	T2	T3
GPT-Image-1	88.33	97.01	97.96	31.11	40.68	50.00	11.27	18.52	18.18	98.39	94.44	91.30
Nano Banana	83.33	86.36	81.25	20.00	47.37	45.24	23.19	9.62	10.91	96.67	94.44	90.00
Gemini 2.0 Flash	90.32	94.29	96.30	21.15	28.57	31.91	10.96	7.14	10.00	86.15	83.64	80.56
Qwen-Image-Edit	98.44	92.86	72.22	21.15	34.92	33.33	12.33	1.72	0.00	98.46	80.00	77.78
Step1X-Edit	60.94	51.43	44.44	13.46	31.75	27.08	0.00	1.72	1.67	87.69	87.27	83.33
FLUX.1-Kontext-dev	50.00	41.43	27.78	15.38	26.98	33.33	0.00	1.72	5.00	90.77	80.00	77.78
OmniGen	29.69	35.71	18.52	17.31	22.22	20.83	5.48	5.17	0.00	76.92	56.36	56.94
AnyEdit	3.12	10.00	11.11	21.15	25.40	27.08	0.00	1.72	1.67	56.92	40.00	52.78
UltraEdit	28.12	15.71	7.41	21.15	36.51	35.42	5.48	6.90	5.00	75.38	38.18	43.06
MagicBrush	7.81	12.86	3.70	19.23	15.87	20.83	0.00	0.00	3.33	43.08	34.55	43.06
IP2P	1.56	8.57	5.56	13.46	15.87	25.00	1.37	0.00	5.00	47.69	20.00	31.94

Table 8: Image rates, overall task rates, and marginal means across three turns (complex mode).

Model	Image Success Rate			Overall Task Rate			Marginal Task Rate		
	T1	T2	T3	T1	T2	T3	T1	T2	T3
GPT-Image-1	73.08	48.45	28.78	73.08	69.77	68.25	73.08	69.98	70.19
Nano Banana	71.46	46.56	28.14	71.46	68.83	67.27	71.46	69.03	67.21
Gemini 2.0 Flash	67.43	40.63	21.89	67.43	64.54	61.94	67.43	64.80	62.17
Qwen-Image-Edit	72.90	46.15	27.62	72.90	69.23	68.07	72.90	67.83	67.66
Step1X-Edit	61.36	32.34	15.73	61.36	57.69	55.01	61.36	55.77	54.02
FLUX.1-Kontext-dev	60.14	33.74	19.58	60.14	59.53	57.87	60.14	57.52	56.99
OmniGen	54.55	23.43	11.01	54.55	50.96	49.83	54.55	48.95	47.90
AnyEdit	39.86	10.31	2.80	39.86	34.79	34.27	39.86	31.47	31.64
UltraEdit	50.70	22.03	8.22	50.70	48.34	46.62	50.70	47.73	47.38
MagicBrush	42.13	14.86	4.55	42.13	38.46	38.81	42.13	38.64	39.34
IP2P	37.24	12.41	2.80	37.24	37.76	35.14	37.24	38.46	34.62

Table 9: Success rates (%) for five instruction types across three turns (complex mode).

Model	Subject Replace			Subject Remove			Material Alter			Color Alter			Subject Add		
	T1	T2	T3	T1	T2	T3	T1	T2	T3	T1	T2	T3	T1	T2	T3
GPT-Image-1	82.22	80.65	78.99	70.31	63.87	58.54	96.49	90.20	84.66	100.00	97.27	91.88	81.67	70.73	69.00
Nano Banana	91.67	88.89	79.33	67.16	55.83	59.88	92.59	85.15	83.33	97.87	98.15	94.19	69.84	71.21	67.77
Gemini 2.0 Flash	85.19	82.88	75.90	57.33	55.56	54.15	93.94	75.00	74.87	100.00	96.90	93.01	70.15	65.97	66.67
Qwen-Image-Edit	87.04	86.49	80.72	70.67	58.33	54.63	93.94	86.21	85.64	100.00	99.22	98.39	77.61	75.69	73.84
Step1X-Edit	90.74	84.68	76.51	52.00	41.67	42.93	93.94	82.76	79.26	100.00	93.02	90.86	64.18	59.03	54.01
FLUX.1-Kontext-dev	85.19	82.88	74.10	54.67	47.92	40.00	86.36	75.00	76.06	100.00	99.22	98.39	67.16	68.75	63.29
OmniGen	88.89	82.88	75.90	46.67	39.58	41.95	86.36	73.28	72.34	100.00	96.12	93.01	53.73	48.61	49.37
AnyEdit	66.67	58.56	49.40	33.33	20.14	22.44	77.27	76.72	70.21	78.57	68.99	72.04	28.36	22.92	21.10
UltraEdit	88.89	87.39	78.31	26.67	30.56	31.71	87.88	79.31	77.66	98.21	93.02	90.32	38.81	46.53	43.46
MagicBrush	83.33	74.77	69.28	28.00	27.78	29.27	83.33	69.83	73.94	92.86	84.50	83.87	37.31	35.42	32.91
IP2P	75.93	73.87	61.45	25.33	31.25	24.88	71.21	63.79	59.57	87.50	82.95	79.03	23.88	31.94	29.11

Table 10: Success rates (%) for four instruction types across three turns (complex mode).

Model	Text Change			Position Change			Count Change			Background Change		
	T1	T2	T3	T1	T2	T3	T1	T2	T3	T1	T2	T3
GPT-Image-1	87.50	92.24	93.75	30.95	22.11	25.36	13.11	10.38	13.12	98.15	96.08	93.37
Nano Banana	84.21	85.34	84.24	24.44	26.00	22.54	20.34	14.15	13.75	98.15	93.40	93.71
Gemini 2.0 Flash	85.94	86.57	84.04	17.31	23.68	16.67	11.11	10.77	6.84	90.77	84.17	80.73
Qwen-Image-Edit	98.44	97.01	93.62	21.15	22.61	24.54	12.33	3.05	3.66	98.46	95.83	93.75
Step1X-Edit	57.81	59.70	52.13	15.38	21.74	25.15	1.37	3.05	1.57	86.15	80.00	73.44
FLUX.1-Kontext-dev	50.00	48.51	47.87	15.38	26.96	27.61	0.00	1.53	3.66	90.77	90.00	88.54
OmniGen	28.12	32.84	27.13	15.38	21.74	17.18	6.85	1.53	2.09	75.38	70.00	69.79
AnyEdit	3.12	5.22	7.98	25.00	26.96	29.45	1.37	1.53	1.57	56.92	44.17	40.62
UltraEdit	29.69	16.42	11.70	21.15	26.09	22.70	5.48	2.29	3.14	75.38	65.00	64.06
MagicBrush	7.81	4.48	6.38	19.23	22.61	17.18	0.00	0.00	5.24	43.08	36.67	35.42
IP2P	3.12	5.22	6.38	13.46	20.00	20.25	1.37	2.29	1.57	47.69	37.50	38.54

Table 11: Consistency scores (%) across DINOv3-based and L1-based object/background metrics. (multi-turn mode)

Model	Object DINOv3 Consistency			Background DINOv3 Consistency			Object $1-L_1$ Consistency			Background $1-L_1$ Consistency		
	T1	T2	T3	T1	T2	T3	T1	T2	T3	T1	T2	T3
GPT-Image-1	73.26	68.80	67.21	88.74	86.76	83.78	79.65	78.32	77.60	78.07	76.53	75.79
Nano Banana	90.17	85.25	84.38	97.65	95.70	94.58	92.39	90.00	89.10	95.95	94.70	93.88
Gemini 2.0 Flash	85.53	77.12	72.02	95.63	93.07	89.74	90.72	86.32	84.11	95.04	93.15	91.73
Qwen-Image-Edit	77.12	71.56	68.51	91.31	89.47	87.45	83.48	79.15	76.32	84.57	81.18	78.43
Step1X-Edit	88.17	81.65	77.33	97.34	95.40	93.09	93.92	90.64	88.80	98.24	97.10	95.73
FLUX.1-Kontext-dev	92.66	87.92	85.29	97.97	96.55	95.14	94.39	91.59	89.91	96.36	95.06	94.13
OmniGen	88.34	80.77	73.64	97.66	96.08	94.21	93.87	91.02	89.43	97.44	97.00	96.34
AnyEdit	82.02	73.41	63.04	90.82	84.42	77.17	92.52	88.96	84.97	93.72	89.98	86.05
UltraEdit	78.81	75.11	72.24	94.80	93.89	92.57	91.86	90.47	89.65	97.12	96.62	96.19
MagicBrush	79.70	70.71	65.46	94.22	91.81	88.27	91.13	87.13	85.56	96.31	94.52	92.87
IP2P	68.24	56.83	48.01	85.47	79.89	72.59	84.44	79.74	77.21	91.31	87.21	83.51

Table 12: Consistency and $1-L_1$ metrics across three turns (multi-turn mode for square image).

Model	Object DINOv3 Consistency (Mean)			Background DINOv3 Consistency			Object L_1 Consistency (Mean)			Background L_1 Consistency		
	T1	T2	T3	T1	T2	T3	T1	T2	T3	T1	T2	T3
GPT4o	73.62	71.27	67.27	90.00	85.72	82.16	80.33	78.80	79.88	85.69	81.86	80.85
nano	88.68	85.19	83.31	96.88	93.79	92.41	89.73	87.64	88.48	94.21	93.77	93.36
Gemini	84.16	79.91	71.13	91.50	91.83	87.07	88.98	87.07	85.13	95.19	93.35	93.34
QWEN	75.36	72.68	68.85	88.50	88.98	82.71	81.66	78.47	77.04	91.16	87.85	85.78
StepEdit	87.40	84.03	78.27	97.43	92.42	88.15	93.14	91.57	89.40	98.10	97.12	96.01
FLUX	92.55	88.92	84.04	96.49	93.57	92.19	92.83	90.61	88.34	96.91	95.74	94.73
OmniGen	89.41	84.51	77.77	97.34	93.13	86.64	93.26	91.48	89.53	95.79	96.44	95.36
AnyEdit	82.25	72.40	53.59	86.12	78.60	70.09	92.33	88.00	82.10	94.36	91.68	87.55
UltraEdit	79.43	76.51	71.54	92.83	89.88	86.54	91.74	90.16	89.24	95.87	95.14	94.63
MagicBrush	79.02	75.60	70.07	92.07	87.33	81.08	89.67	87.53	86.90	95.29	93.88	92.38
IP2P	76.38	66.12	54.94	85.29	81.46	65.50	86.90	82.25	77.79	92.45	88.01	84.51

Table 13: Consistency and L_1 metrics across three turns (multi-turn model for unsquared image).

Model	Object DINOv3 Consistency (Mean)			Background DINOv3 Consistency			Object $1-L_1$ Consistency (Mean)			Background $1-L_1$ Consistency		
	T1	T2	T3	T1	T2	T3	T1	T2	T3	T1	T2	T3
GPT4o	73.22	68.53	67.20	88.60	86.88	83.99	79.57	78.27	77.35	77.20	75.91	75.14
nano	90.34	85.26	84.50	97.74	95.94	94.88	92.69	90.29	89.17	96.16	94.81	93.95
Gemini	85.69	76.79	72.12	96.14	93.23	90.10	90.91	86.23	83.99	95.02	93.12	91.51
QWEN	77.32	71.43	68.47	91.65	89.53	88.10	83.68	79.23	76.23	83.78	80.37	77.43
StepEdit	88.26	81.37	77.22	97.33	95.77	93.77	94.01	90.53	88.73	98.26	97.09	95.70
FLUX	92.67	87.80	85.44	98.15	96.92	95.54	94.57	91.70	90.10	96.30	94.98	94.05
OmniGen	88.22	80.33	73.14	97.70	96.45	95.25	93.94	90.97	89.42	97.64	97.07	96.47
AnyEdit	82.00	73.53	64.18	91.39	85.14	78.14	92.54	89.07	85.31	93.64	89.78	85.84
UltraEdit	78.74	74.95	72.32	95.04	94.39	93.40	91.87	90.51	89.70	97.26	96.80	96.40
MagicBrush	79.78	70.14	64.90	94.48	92.37	89.27	91.30	87.08	85.40	96.44	94.59	92.94
IP2P	67.32	55.75	47.18	85.50	79.69	73.57	84.17	79.45	77.14	91.18	87.12	83.38

Table 14: Consistency scores (%) across object/background DINOv3 and L_1 metrics (complex mode).

Model	Object DINOv3			Object $1-L_1$			Background DINOv3			Background $1-L_1$		
	T1	T2	T3	T1	T2	T3	T1	T2	T3	T1	T2	T3
GPT-Image-1	73.23	70.02	67.57	79.52	78.03	77.29	88.72	86.77	84.79	77.96	77.38	76.51
Nano Banana	89.23	87.20	86.46	92.15	91.08	90.40	97.39	96.69	95.38	96.39	95.75	95.33
Gemini 2.0 Flash	85.41	80.37	77.38	90.60	88.45	86.53	96.03	94.18	92.83	95.03	94.77	93.46
Qwen-Image-Edit	77.12	76.09	76.69	83.48	83.08	83.11	91.31	91.32	90.51	84.57	84.93	85.35
Step1X-Edit	88.14	85.31	84.38	93.93	92.34	92.11	97.34	96.37	95.44	98.24	98.02	98.04
FLUX.1-Kontext-dev	92.66	90.30	89.19	94.39	92.79	91.61	97.97	96.74	95.40	96.36	95.57	94.04
OmniGen	88.37	85.15	83.14	93.88	92.46	91.06	97.62	97.10	96.07	97.45	97.58	97.40
AnyEdit	81.90	82.94	84.92	92.34	92.43	93.72	90.97	92.63	93.78	94.15	95.11	95.87
UltraEdit	78.81	72.75	71.67	91.86	89.51	88.99	94.80	93.01	92.03	97.12	96.35	96.02
MagicBrush	79.70	75.64	75.53	91.13	89.23	88.69	94.22	94.34	93.13	96.31	96.14	95.83
IP2P	68.24	67.31	69.49	84.44	82.93	83.72	85.47	85.88	86.45	91.31	89.94	90.19

Table 15: Human preference scores, p999, and p99 across three turns (multi-turn mode).

Model	Human Preference Score			p999			p99		
	T1	T2	T3	T1	T2	T3	T1	T2	T3
GPT-Image-1	6.6519	6.5898	6.5609	84.73	82.96	82.50	74.38	71.91	70.54
Nano Banana	4.9431	5.1179	5.2638	89.67	90.27	90.56	81.31	82.01	82.09
Gemini 2.0 Flash	4.4386	4.2332	4.0677	90.95	92.21	92.95	83.08	84.79	86.24
Qwen-Image-Edit	5.8591	5.7198	5.1502	89.16	97.20	99.04	79.60	90.51	95.28
Step1X-Edit	4.0577	3.3443	2.7569	92.81	95.39	97.27	85.10	88.46	91.21
FLUX.1-Kontext-dev	5.1192	5.0701	5.0354	90.76	91.94	93.21	82.05	83.03	84.58
OmniGen	4.6099	4.0743	3.4958	93.15	95.24	96.71	85.55	88.24	90.50
AnyEdit	3.6609	2.8017	1.9457	86.70	86.70	86.71	77.54	76.53	75.82
UltraEdit	4.7934	4.6806	4.3598	92.71	94.19	95.82	85.42	86.76	88.34
MagicBrush	3.8465	3.0805	2.3606	91.49	93.33	94.20	83.42	84.70	85.32
IP2P	3.2020	2.3779	1.4418	89.61	91.59	92.44	81.79	83.78	84.77

Table 16: Updated human preference scores, p999 scores, and p99 scores across three turns (complex mode).

Model	Human Preference Score			p999			p99		
	T1	T2	T3	T1	T2	T3	T1	T2	T3
GPT-Image-1	6.6328	6.8428	6.9655	85.33	84.14	84.44	74.73	73.92	73.07
Nano Banana	4.9444	5.1700	5.3632	89.65	90.67	91.79	81.02	81.93	82.75
Gemini 2.0 Flash	4.4511	4.5428	4.5732	91.27	92.66	93.48	83.85	85.69	86.75
Qwen-Image-Edit	5.8591	5.8769	5.9155	89.16	90.92	92.23	79.60	81.36	82.62
Step1X-Edit	4.0534	3.9063	3.8648	92.82	93.55	94.05	85.11	85.49	86.01
FLUX.1-Kontext-dev	5.1192	5.2446	5.4645	90.76	91.01	91.29	82.05	81.53	81.55
OmniGen	4.5976	4.3070	3.8122	93.15	93.74	95.65	85.56	86.28	88.57
AnyEdit	3.7020	3.7601	3.8382	86.47	87.16	87.43	77.82	78.60	79.12
UltraEdit	4.7934	4.7647	4.8117	92.71	93.06	93.24	85.42	86.09	86.47
MagicBrush	3.8465	3.6029	3.5523	91.49	91.52	91.64	83.42	83.31	83.07
IP2P	3.2020	3.3552	3.5640	89.61	90.46	90.86	81.79	82.57	82.71

(a) Visual quality (Qwen2.5-VL: 60, HPSv3: 1.61).

(b) Visual quality (Qwen2.5-VL: 60, HPSv3: 3.35).

Figure 12: **Examples of visual quality evaluation.** Scores are reported from both VLM Qwen2.5-VL and HPSv3 for comparison. The VLM score ranges from 0 to 100, so the VLM gives a *positive* score to both images with significant artifacts.

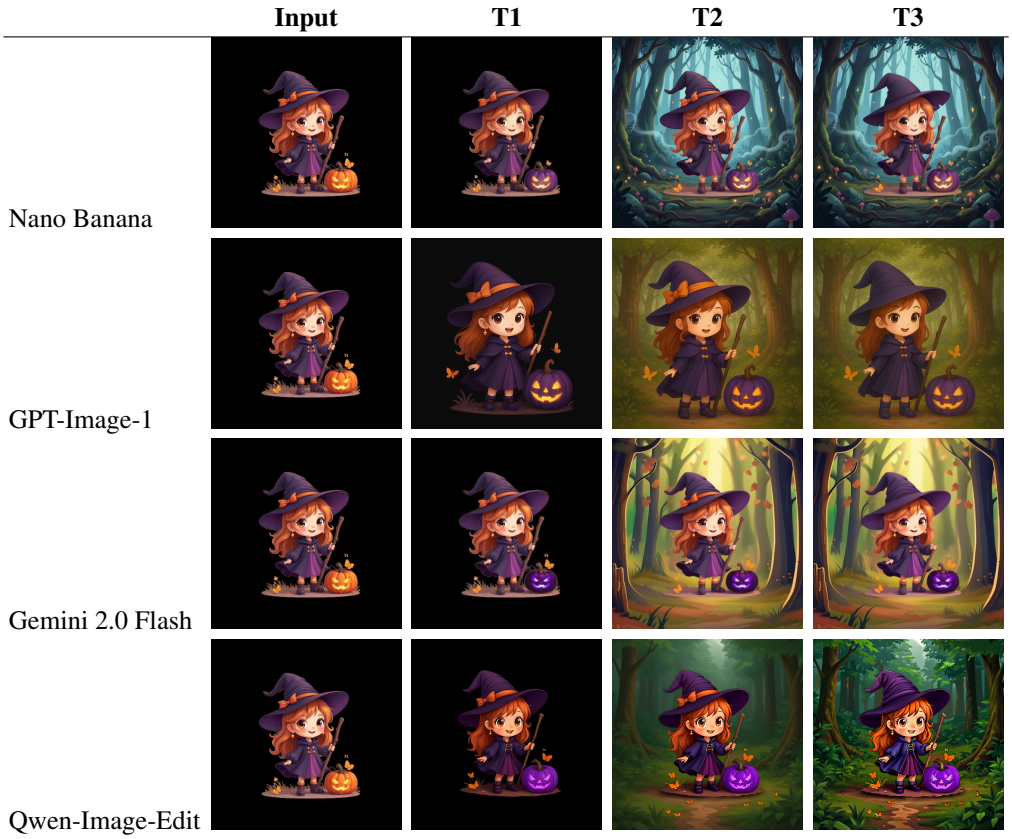

Figure 13: **T1: Change the color of pumpkin to purple; T2: Change the background to forest; T3: Remove fabric orange bow.** Row-wise quality examples for the first four models: Nano Banana, GPT-Image-1, Gemini 2.0 Flash, and Qwen-Image-Edit. Each row shows generations for Input and three editing turns.

E More Quality Examples

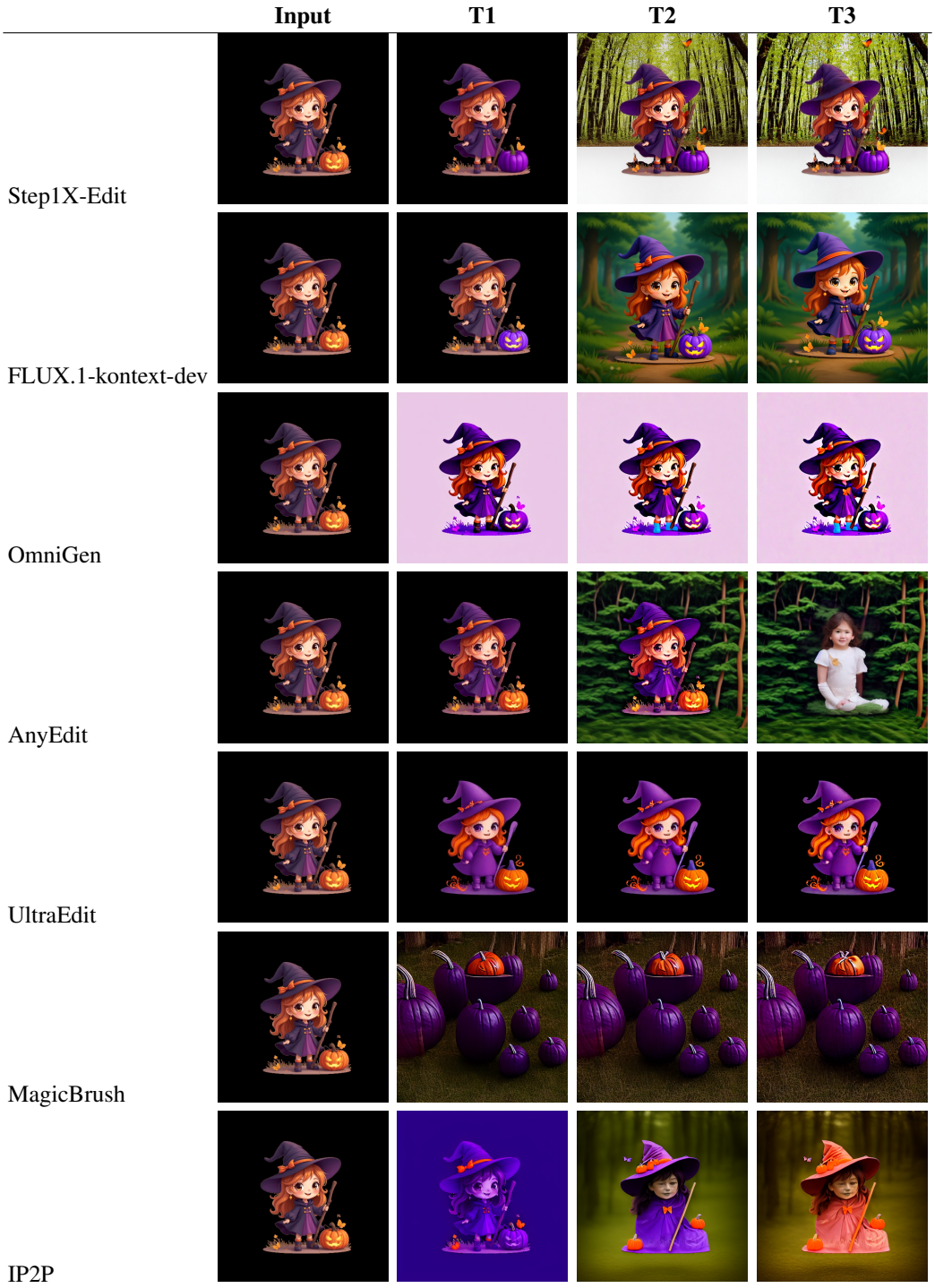

Figure 14: **T1: Change the color of pumpkin to purple; T2: Change the background to forest; T3: Remove fabric orange bow.** Row-wise quality examples for the remaining models: Step1X-Edit, FLUX.1-kontext-dev, OmniGen, AnyEdit, UltraEdit, MagicBrush, and IP2P.